

A continuous-discontinuous model for crack branching

Elena Tamayo-Mas¹ | Jordi Feliu-Fabà² | Montserrat Casado-Antolin³ | Antonio Rodríguez-Ferran³

¹British Geological Survey, Environmental Science Centre, Nicker Hill, Keyworth, Nottingham, United Kingdom

²Institute for Computational and Mathematical Engineering, Stanford University, California, USA

³Laboratori de Càlcul Numèric (LaCàN), Universitat Politècnica de Catalunya, BarcelonaTech, Barcelona, Spain

Correspondence

Antonio Rodríguez-Ferran, Campus Diagonal Nord UPC, Edifici C2, C. Jordi Girona 1-3, 08034 Barcelona, Spain
Email: antonio.rodriguez-ferran@upc.edu

Funding information

Spanish Ministry of Economy and Competitiveness (Grant number: DPI2016-74929-R); Generalitat de Catalunya (Grant number: 2017SGR1278)

A new continuous-discontinuous model for fracture that accounts for crack branching in a natural manner is presented. It combines a gradient-enhanced damage model based on non-local displacements to describe diffuse cracks and the extended finite element method (X-FEM) for sharp cracks. Its most distinct feature is a global crack tracking strategy based on the geometrical notion of medial axis: the sharp crack propagates following the direction dictated by the medial axis of a damage isoline. This means that, if the damage field branches, the medial axis automatically detects this bifurcation and a branching sharp crack is thus easily obtained. In contrast to other existing models, no special crack-tip criteria are required to trigger branching. Complex crack patterns may also be described with this approach, since the X-FEM enrichment of the displacement field can be recursively applied by adding one extra term at each branching event. The proposed approach is also equipped with a crack-fluid pressure, a relevant feature in applications such as hydraulic fracturing or leakage-related events. The capabilities of the model to handle propagation and branching of cracks are illustrated by means of different two-dimensional numerical examples.

KEYWORDS

crack branching; gradient damage; medial axis; fracture; finite

1 | INTRODUCTION

In many applications, one may use a continuous model based on damage mechanics, with a diffuse (i.e. smeared) representation of cracks. This is the case if the goal of the analysis is to model damage inception and the progressive stiffness degradation and loss of load-carrying capacity. In other applications, dating back to classical fracture mechanics, a sharp (i.e. explicit) representation of cracks is preferred. Continuous-discontinuous models are becoming increasingly popular in computational fracture mechanics. The goal is to put together into a combined approach the strong features of these two classical viewpoints, damage and fracture mechanics.

Many recent continuous-discontinuous models are capable of capturing a crack that propagates along a path not known in advance. With only a few exceptions, however, these models do not handle complex crack patterns in a natural manner. The modelling of a branching crack poses specific challenges, such as the fact that the model needs to decide when a propagating crack branches into two distinct cracks, possibly in a recursive manner. The explicit representation of a (branching) crack may be convenient for a number of reasons. It allows, for instance, to compare experimental and numerical crack opening displacements, or to take into account the relative orientation between the crack faces and the fibres in the simulation of fibre-reinforced concrete. Consider also applications related to hydraulic fracturing or leakage in concrete structures. In these processes, cracks are filled with a pressurised fluid whose hydraulic pressure depends on the shape of the crack.

The goal of this paper is to present a continuous-discontinuous model that handles branching in a natural way, without resorting to any ad-hoc branching criteria. The model is also equipped with the capability of injecting a pressurised fluid into the cracks.

An outline of this paper follows. The remainder of this introduction briefly reviews continuous-discontinuous models of fracture (section 1.1) and the physics and modelling of crack branching (section 1.2). The proposed model is described in section 2. The starting point is a continuous-discontinuous model for non-branching cracks [1, 2] that is briefly reviewed in section 2.1. The improvement of this model to account for branching cracks and crack-fluid pressure is discussed in sections 2.2 and 2.3 respectively. Such new capabilities are illustrated in section 3 by means of several numerical examples. The concluding remarks of section 4 close the paper.

1.1 | Overview of continuous-discontinuous models of fracture

In continuous-discontinuous models, diffuse and sharp crack representations coexist. Crack inception and the initial stages of propagation are represented in a diffuse way by means of a continuous model. Later in the analysis, when dictated by a switching criterion, a sharp discontinuity is injected. Designing a continuous-discontinuous model amounts to making the following four decisions:

1. *How to model diffuse cracks* by means of a continuous model. Typical choices are integral-type [3] or gradient-enriched [4] non-local continuum damage models, and phase-field approaches [5, 6].
2. *When to switch from a diffuse crack to a sharp crack*. This transition may be controlled by a damage threshold [1, 2, 7, 8, 9] or energetic considerations [10, 11, 12], for instance.
3. *Where to locate the sharp crack*. Crack tracking techniques may be local (that is, based on crack-tip strain/stress fields) [10, 13, 14, 15] or global (that is, based on the background damage field in a neighbourhood of the crack

tip) [1, 2, 12].

4. *How to model sharp cracks.* This refers both to the mechanical model (traction-free cracks vs cohesive cracks equipped with a traction-separation law) and to the discretisation of the discontinuous displacement fields, either with a fitted mesh and node duplication (cohesive zone model, CZM [11]) or an unfitted mesh. Unfitted techniques consist either on a global nodal enrichment (extended finite element method, X-FEM [16, 17]) or a local element-based enrichment of the displacement field (strong discontinuity approach, SDA [18]).

In their pioneering work, Mazars and Pijaudier-Cabot [19] establish the thermodynamic link between the two classical theories, by showing that it is possible to obtain the fracture energy from a non-local damage model and vice versa. Jirásek and Zimmermann [13] combine smeared cracks for the early stages of material degradation with embedded discontinuities after strain reaches a critical value. Wells et al. [20] use the partition of unity concept to couple a softening viscoplasticity model with traction-free discontinuities. Simone et al. [14] replace viscoplasticity by a gradient-enhanced continuum damage model and choose the direction of maximum accumulation of non-local equivalent strain for crack propagation. Seabra et al. [21] propose a continuous-discontinuous model where a non-local integral damage formulation is used to determine the direction and length of a traction-free discontinuity. In these approaches, a traction-free crack is introduced when the inelastic bulk is fully degraded. Comi et al. [7] define a critical damage $D_{\text{crit}} < 1$ as switching criterion, and combine the not fully degraded bulk with an energetically equivalent cohesive crack. Similar energetic considerations are made by Cazes et al. for elastic-damage models [22] and for damage-plasticity [23], and by Cuvilliez et al. [24].

Benvenuti and Tralli [25] propose the regularised extended finite element approach (Re-XFEM), in which cracks are represented first by means of a continuous damage approach, later by a regularised discontinuous approach (Re-XFEM) and finally by a purely discontinuous strategy, where the standard X-FEM is retrieved.

Recently, various continuous-discontinuous models with additional features have been proposed. Roth et al. [10] use a regularised local anisotropic continuum damage model for the first stages of fracture process zone formation and a stress-based integral-type non-local damage model [26] for crack tracking. The transition from continuum damage to cohesive X-FEM cracks is based on energetic considerations. The sharp crack grows perpendicularly to the maximum non-local principal stress and crosses all finite elements above a critical damage. The interpenetration of crack surfaces is avoided by means of a penalty term.

The approach of Wang and Waisman [9] is also based on the combination of an integral-type non-local damage model and cohesive cracks, in this case represented by means of discrete springs. The displacement jump across the sharp cracks is discretised with the X-FEM. The continuous-to-discontinuous transition, at a critical damage level, is based on energetic considerations. The crack grows in the direction of maximum bulk damage, and the increment of crack length is a user-defined parameter. Interestingly, the damage field is frozen in the wake of the sharp crack. The interpenetration of crack surfaces is avoided by means of a penalty term in the spring mechanics.

The main ingredients in the proposal of Bobiński and Tejchman [27] are a non-local softening model (elastoplasticity or isotropic damage) and energetically equivalent X-FEM sharp cracks. The continuous-to-discontinuous transition takes place when the hardening/softening parameter (for elastoplasticity) or a damage history parameter (damage) exceeds a threshold. In order to prevent locking or a delay in the crack growth, this condition is not only checked at the crack tip but also in all the integration points lying inside a specific circular window.

Lé et al. [11] propose a continuous-discontinuous model based on the combination of the Thick Level Set (TLS) [28] with the cohesive zone model. The two key ideas are to express the traction-separation law of the CZM in terms of an interfacial damage field, and to describe this interfacial damage and the bulk TLS damage by means of the same level set function. This is done by means of careful energetic considerations to enforce equivalence in a

one-dimensional setting.

Other recent proposals are based on the phase-field framework. The *Xfield* method of Giovanardi et al. [15] uses the phase-field approach around the crack-tip to model crack propagation in a diffuse way. In the wake of the crack tip, the X-FEM is used to model a sharp discontinuity in an elastic bulk. A key ingredient of this approach is the boundary conditions in the phase-field window around the crack tip. The crack tip location is determined by means of a *local* criterion based on the maximum gradient of the phase field in the direction of crack propagation (see the discussion on local vs. global crack tracking in section 2.1.2).

The proposal of Geelen et al. [12] is also based on the combination of phase-field and X-FEM. The two main distinct features are a crack length functional that triggers the continuous-to-discontinuous transition when the increment of diffuse crack length reaches a prescribed value, and an optimisation-based *global* crack tracking strategy that consists in fitting the actual damage field provided by the phase-field model and an auxiliary geometrical damage field that can be thought of as a diffuse crack.

All the models cited above are based on the finite element method. Approaches based on alternative discretisation techniques can also be found. Wu et al. [29], for instance, propose a meshfree continuous-discontinuous approach for dynamic ductile fracture, based on the combination of a gradient-enriched damage model with a visibility criterion [30] for sharp cracks, whereas the meshfree approach of Wang et al. [31] for brittle solids is based on the peridynamic theory. Peridynamics grids are also used by Zaccariotto et al. [32], who combine them with the standard finite element method to describe crack propagation phenomena.

1.2 | Crack branching

A propagating crack may branch for a number of reasons. In dynamics, energetic considerations play a crucial role. Each branching event can be regarded as the generation of an additional crack tip, so that more energy can be dissipated [33, 34]. An important –albeit still debated– notion in dynamic fracture mechanics is that of critical crack tip velocity [33, 35], above which a crack tends to branch. In quasistatics, the key ingredient of branching is heterogeneity. In heterogeneous media, holes (or soft inclusions) act as crack attractors, whereas stiffer inclusions tend to repel them [34]. Both in statics and in dynamics, the crack and heterogeneity patterns are related [34].

A key ingredient of any computational model for fracture that aims to capture complex crack patterns is a *branching criterion*. That is, a mechanism to trigger crack bifurcation. If an elastic background continuum model is assumed, the crack-tip velocity [35] or the energy release rate [36] may be used as branching criteria. If, on the other hand, an inelastic non-local continuum model is chosen, such as gradient-enriched damage models or phase-field approaches, an extrinsic branching criterion is not required since such models naturally capture branching, both in statics [1, 2, 12, 37] and in dynamics [34, 38].

Any continuous-discontinuous (or purely discontinuous, i.e. based on an elastic continuum) model of branching also requires a way to numerically represent the bifurcation of a sharp discontinuity. Like for the simpler case of a single, non-branching crack, this may be done by means of either fitted or unfitted meshes. Regarding the former, the cohesive finite element method has amply demonstrated its capability to capture complex crack patterns (see, for instance, the work of Arias et al. [39] and references therein), at the expense of some mesh dependency of the crack geometry and the need of very fine meshes. Regarding the latter, only a few unfitted continuous-discontinuous (or purely discontinuous) models of fracture exhibit branching capabilities.

In their pioneering work, Daux et al. [40] extended the then recent X-FEM formulation to account for branching cracks by employing additional enrichment functions. *The material regions* approach of Richardson et al. [41] is based on the combination of X-FEM and an algorithm for cutting triangulated domains. Since the focus is on the geometrical

and discretisation aspects, branching criteria are not discussed in these two works.

The discontinuous model of Linder and Armero [35] for dynamic crack branching in brittle materials is based on embedded strong discontinuities. When the crack-tip velocity reaches a critical threshold velocity, branching occurs. The incoming crack branches at the centre of the corresponding finite element. The two new branches propagate in opposite normal directions, so a T-shaped crack pattern is obtained. In the spirit of the strong discontinuity approach [18], the displacement jumps in the branching element are defined by means of a branching separation mode, and the associated degrees of freedom are statically condensed.

The approach of Lloberas-Valls et al. [36] combines weak and strong discontinuity injections to describe dynamic fracture. In their model, branching is explained from an energetic point of view. The region of crack branching is enhanced with a weak displacement discontinuity, whereas the rest of the crack is modelled with a strong discontinuity. In contrast with the model of Linder and Armero [35], no special elements with branched strong discontinuities are required.

The continuous-discontinuous model of Geelen et al. [12] described in section 1.1 also handles crack branching. In order to do so, the sharp crack insertion algorithm makes an initial guess of *two* (rather than only one) new sharp segments. If the angle between the two optimal segments is above a threshold, branching is assumed; if not, the two segments are collapsed into one.

2 | MODEL FORMULATION

Our starting point is the continuous-discontinuous model for fracture with geometrical crack tracking, based on the medial-axis concept, presented by Tamayo-Mas and Rodríguez-Ferran [1, 2, 8]. This model is briefly reviewed in section 2.1. In those references, various two- and three-dimensional examples of propagating (non-branching) cracks are shown. The remainder of section 2 describes the two new features of this contribution: the X-FEM enrichment of the displacement field to account for crack branching in section 2.2 and the inclusion of crack-fluid pressure in section 2.3. Standard notation is used. Vector fields in the continuum are represented by slanted boldface type (\boldsymbol{u} : displacement field). Nodal vectors associated to the FE discretisation are denoted by upright boldface type (\mathbf{a} : nodal displacements).

2.1 | A continuous-discontinuous model with geometrical crack tracking

The main ingredients of the continuous-discontinuous model for fracture [1, 2, 8] are: *i*) a gradient-enhanced damage model based on non-local displacements; *ii*) a geometrical crack tracking approach based on the medial axis of the damaged region; *iii*) X-FEM enrichment to insert a discontinuity in the local and non-local displacement fields along the medial axis.

2.1.1 | Gradient-enhanced damage model

The gradient-enhanced damage model is summarised in table 1. It is a two-field formulation that involves two displacement fields: the usual local displacements \boldsymbol{u} and non-local (or smoothed) displacements $\tilde{\boldsymbol{u}}$. Stresses depend on these two displacements via the corresponding strains, see equations (1a)-(1c), where ∇^s denotes the symmetrised gradient. Note that the non-local strains $\tilde{\boldsymbol{\epsilon}}$ drive the damage parameter D .

The model consists of two coupled field equations in the problem domain Ω : the equilibrium equation (1d) –

TABLE 1 Gradient-enhanced damage model based on non-local displacements

Stress definition	$\sigma(\mathbf{u}, \tilde{\mathbf{u}}) = (1 - D(\tilde{\varepsilon}))\mathbf{C} : \varepsilon$	(1a)
Local strains	$\varepsilon = \nabla^s \mathbf{u}$	(1b)
Non-local strains	$\tilde{\varepsilon} = \nabla^s \tilde{\mathbf{u}}$	(1c)
Equilibrium equation	$\nabla \cdot \sigma(\mathbf{u}, \tilde{\mathbf{u}}) = \mathbf{0}$ in Ω	(1d)
Prescribed displacements	$\mathbf{u} = \mathbf{u}^*$ on Γ_u	(1e)
Prescribed tractions	$\sigma \cdot \mathbf{n} = \mathbf{t}^*$ on Γ_t	(1f)
Regularisation equation	$\tilde{\mathbf{u}} - \ell^2 \nabla^2 \tilde{\mathbf{u}} = \mathbf{u}$ in Ω	(1g)
Normal component: Dirichlet	$\tilde{\mathbf{u}} \cdot \mathbf{n} = \mathbf{u} \cdot \mathbf{n}$ on $\partial\Omega$	(1h)
Tangential component: Neumann	$\mathbf{n} \cdot \nabla \tilde{\mathbf{u}} \cdot \boldsymbol{\tau} = \mathbf{n} \cdot \nabla \mathbf{u} \cdot \boldsymbol{\tau}$ on $\partial\Omega$	(1i)

where inertia effects and body forces are neglected— and the regularisation equation (1g). The equilibrium equation is complemented with the usual boundary conditions (1e) and (1f): prescribed displacements \mathbf{u}^* in Γ_u and prescribed tractions \mathbf{t}^* in Γ_t , with $\partial\Omega = \Gamma_u \cup \Gamma_t$. The regularisation (or smoothing) equation, which has the crucial role of injecting the characteristic length ℓ into the formulation, is complemented with the so-called combined boundary conditions [1, 2]: Dirichlet for the normal component of displacements, equation (1h) and Neumann for the tangential component, equation (1i). Vectors \mathbf{n} and $\boldsymbol{\tau}$ represent respectively the outward unit normal and unit tangent to the boundary $\partial\Omega$ of the two-dimensional domain Ω . For a three-dimensional domain Ω , equation (1i) is stated for the two unit tangents, $\boldsymbol{\tau}_1$ and $\boldsymbol{\tau}_2$.

The key difference with respect to other gradient damage models is that the regularisation equation (1g) is expressed in terms of displacements, rather than a state variable [4]. We have argued in [42, 43, 44] that this choice has a number of attractive features, such as straightforward linearisation for Newton iterations, clear meaning of the boundary conditions, and correct damage initiation at the crack tip in pre-cracked specimens.

2.1.2 | Geometrical crack tracking

A key decision in the design of a continuous-discontinuous models is where to locate the sharp crack. We classify the approaches available into two groups: local and global crack tracking strategies. Local approaches are based on information at (or in a small neighbourhood of) the crack tip. Various near-tip field features may be used to decide the direction of crack tracking: maximum principal stress, maximum principal non-local strain [13] or maximum accumulation of non-local equivalent strain [14]. In our view, these local approaches —of a mechanical nature—, make little use of the background continuous model, and this may be regarded as a “waste” of valuable information.

We prefer to use a more global approach, of a geometrical nature. In the medial-axis approach [1, 2], the sharp crack is placed “in the middle” of the damage band defined by the isoline $D = D^*$. This intuitive notion has a precise geometrical definition: the medial axis of a line in \mathbb{R}^2 is the locus of the centres of the interior bi-tangent circles, see

figure 1. This definition can be extended to three dimensions in a natural way: the medial surface of a surface in \mathbb{R}^3 is the locus of the centres of the interior bi-tangent spheres. Various codes to extract the medial axis are available [45, 46].

The discontinuity is inserted along the medial axis when damage reaches a critical value of $D = D_{crit}$. This is done progressively, by checking the damage field at the end of each load step: as soon as $D \geq D_{crit}$ for one or more elements ahead of the crack tip, their nodes are marked for X-FEM enrichment. This results in displacement jumps at the next load step. Either a traction-free crack [2] or a cohesive crack [8] may be inserted. For simplicity, the case of non-cohesive cracks is considered here.

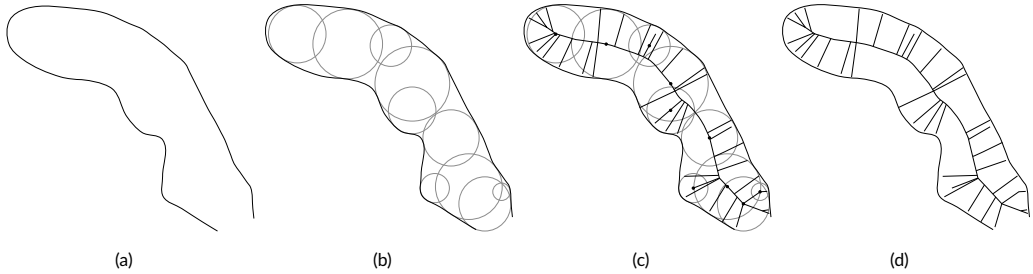


FIGURE 1 Geometrical crack tracking: (a) Given a domain Ω , (b) the bi-tangent interior circles are computed, and (c) joining their centres, (d) the medial axis is obtained. Note that the medial axis is very sensitive to details in the boundary of the object and thus, simplified and stable versions are usually preferred, see section 2.2.1. Figure adapted from [2].

Another global approach is that of Geelen et al. [12]: in the context of a continuous-discontinuous phase-field model, the crack is located by fitting two fields: the mechanical damage phase-field and a geometrical auxiliary damage field, which can be regarded as a diffuse representation of the discontinuity. This fitting is carried out by solving a minimisation problem [47].

2.1.3 | X-FEM enrichment of the displacement fields

The two displacement fields, \mathbf{u} and $\tilde{\mathbf{u}}$, are made discontinuous across the crack by means of the eXtended Finite Element Method [16, 17]. They are represented as

$$\mathbf{u}(\mathbf{x}) = \mathbf{a}(\mathbf{x}) + \psi(\mathbf{x})\mathbf{b}(\mathbf{x}) \tag{2a}$$

$$\tilde{\mathbf{u}}(\mathbf{x}) = \tilde{\mathbf{a}}(\mathbf{x}) + \psi(\mathbf{x})\tilde{\mathbf{b}}(\mathbf{x}) \tag{2b}$$

where $\mathbf{a}(\mathbf{x})$, $\mathbf{b}(\mathbf{x})$, $\tilde{\mathbf{a}}(\mathbf{x})$ and $\tilde{\mathbf{b}}(\mathbf{x})$ are continuous fields and $\psi(\mathbf{x})$ is the sign function (i.e. -1 to $+1$ step) across the discontinuity Γ . In order to describe the jumps, fields $\mathbf{b}(\mathbf{x})$ and $\tilde{\mathbf{b}}(\mathbf{x})$ with a compact support along the discontinuity may be used. In practice, this means that, upon finite element discretisation, only the nodes belonging to elements crossed by the discontinuity are enriched with degrees of freedom \mathbf{b}_J and $\tilde{\mathbf{b}}_J$, whereas all nodes in the mesh have \mathbf{a}_J

and $\tilde{\mathbf{a}}_I$ degrees of freedom, see figure 2. That is, the finite element approximations of the displacement fields are

$$\mathbf{u}(\mathbf{x}) \approx \mathbf{u}^h(\mathbf{x}) = \sum_{I \in \mathbb{I}} N_I(\mathbf{x}) \mathbf{a}_I + \sum_{J \in \mathbb{J} \subseteq \mathbb{I}} N_J(\mathbf{x}) \psi(\mathbf{x}) \mathbf{b}_J \quad (3a)$$

$$\tilde{\mathbf{u}}(\mathbf{x}) \approx \tilde{\mathbf{u}}^h(\mathbf{x}) = \sum_{I \in \mathbb{I}} N_I(\mathbf{x}) \tilde{\mathbf{a}}_I + \sum_{J \in \mathbb{J} \subseteq \mathbb{I}} N_J(\mathbf{x}) \psi(\mathbf{x}) \tilde{\mathbf{b}}_J \quad (3b)$$

where \mathbb{I} is an index set of all nodes in the mesh, \mathbb{J} is an index set of enriched nodes and $N_I(\mathbf{x})$ are the standard finite element shape functions. Note also that if the crack tip is assumed to be in an element edge (and not inside an element), then the nodes in that edge should not be enriched, see figure 2.

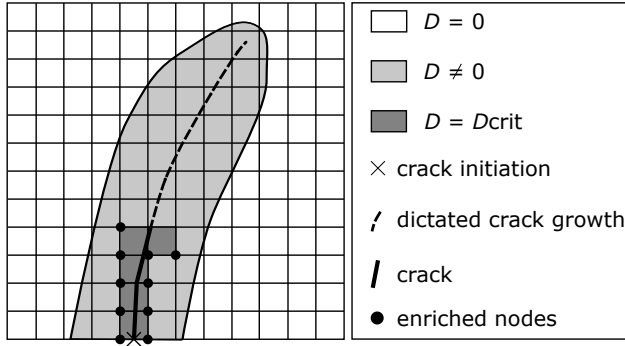


FIGURE 2 Finite element enrichment by means of X-FEM. Figure adapted from [2].

The variational formulation and finite element discretisation of this continuous-discontinuous model is discussed in [1, 2]. The extension to branching cracks is discussed in full detail by Feliu-Fabà [48] and summarised in appendix A.

2.2 | Crack branching

The continuous-discontinuous model reviewed in section 2 is extended here to handle branching cracks. Interestingly, and due to the versatility of the main ingredients of the original approach, only a few modifications are required. The effect of crack branching on the geometrical crack tracking and on the X-FEM enrichment of the displacement fields is discussed in sections 2.2.1 and 2.2.2 respectively. The continuous gradient-enriched damage model of section 2.1.1 applies without any change.

2.2.1 | Geometrical tracking of crack branching

A very appealing feature of the geometrical crack tracking based on the medial axis of section 2.1.2 is that it applies naturally to branching cracks and other complex crack patterns. Indeed, if the damage field of the background continuum model branches (due to the boundary conditions, heterogeneities or any other cause), see figure 3(a), this branching is of course reflected in the damage isoline, so it is captured by the medial axis, see figure 3(b). This is a direct consequence of the generality of the geometrical notion of medial axis. Like in the case of non-branching cracks, we use the so-called θ -simplified medial axis [49] to “prune” the small branches and retain the “spine”, see fig-

ure 3(c). The simplification consists in discarding the circles with a separation angle between tangency points below a prescribed angle θ . Note that, in contrast with other approaches for branching [35], no specific tip criteria are required to trigger branching, neither for the diffuse crack nor for the sharp crack.

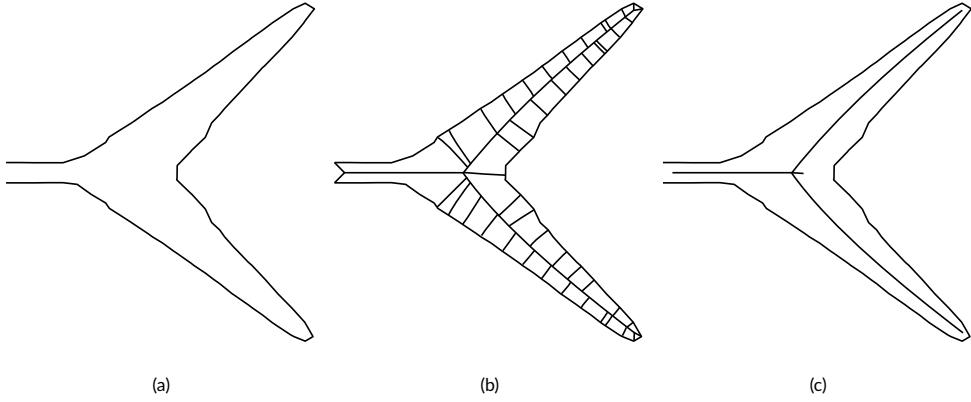


FIGURE 3 The medial axis of a branching crack: (a) damage isoline; (b) medial axis; (c) simplified medial axis. Figure adapted from [2].

2.2.2 | X-FEM enrichment for crack branching

The X-FEM enrichment of section 2.1.3 can be extended in a straightforward manner to multiple cracks [40]. Let us consider first the case of one branching crack, see figure 4. The crack is understood as a primary crack Γ_1 and a secondary crack Γ_2 . The discontinuous displacement fields are represented as

$$\mathbf{u}(\mathbf{x}) = \mathbf{a}(\mathbf{x}) + \psi_1(\mathbf{x})\mathbf{b}_1(\mathbf{x}) + \psi_2(\mathbf{x})\mathbf{b}_2(\mathbf{x}) \tag{4a}$$

$$\tilde{\mathbf{u}}(\mathbf{x}) = \tilde{\mathbf{a}}(\mathbf{x}) + \psi_1(\mathbf{x})\tilde{\mathbf{b}}_1(\mathbf{x}) + \psi_2(\mathbf{x})\tilde{\mathbf{b}}_2(\mathbf{x}) \tag{4b}$$

where $\psi_1(\mathbf{x})$ and $\psi_2(\mathbf{x})$ are the sign functions across the discontinuities Γ_1 and Γ_2 respectively. Note that the labelling of one of the two branches (in the case of figure 4, the right one) as secondary crack is arbitrary. One could label alternatively the left branch as the secondary crack, or even treat the “trunk” and the two branches as three different cracks. What is relevant is to ensure the jumps across the Y pattern.

The fact that the discontinuous displacement fields now have two enrichment terms rather than only one, cf. equations (3) and (4), must be reflected both in the variational formulation and in the finite element discretisation, as discussed in appendix A.

For the case of a more complex branch pattern as the one depicted in figure 5, equation (4) is extended into

$$\mathbf{u}(\mathbf{x}) = \mathbf{a}(\mathbf{x}) + \sum_{i=1}^{n\text{cracks}} \psi_i(\mathbf{x})\mathbf{b}_i(\mathbf{x}) \tag{5a}$$

$$\tilde{\mathbf{u}}(\mathbf{x}) = \tilde{\mathbf{a}}(\mathbf{x}) + \sum_{i=1}^{n\text{cracks}} \psi_i(\mathbf{x})\tilde{\mathbf{b}}_i(\mathbf{x}) \tag{5b}$$

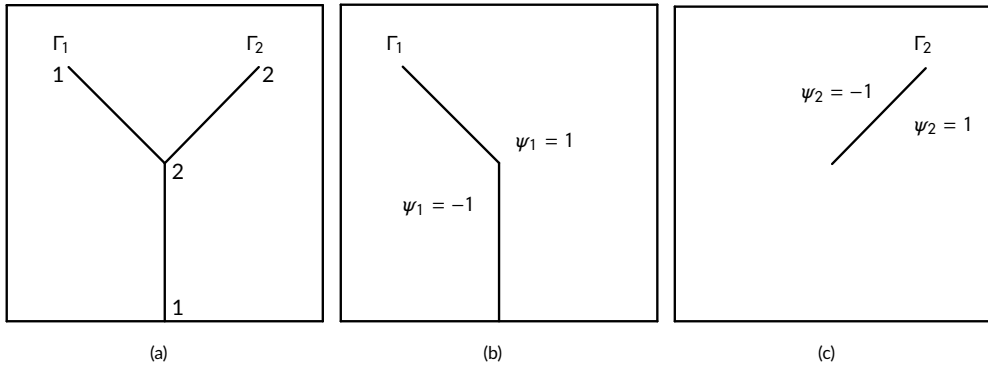


FIGURE 4 X-FEM enrichment: (a) a branching crack is modelled as (b) a primary crack and (c) a secondary crack. The numbers in (a) indicate the two endpoints of each crack.

where i is a crack counter that spans all the cracks, and $\psi_i(x)$ for $i = 1, \dots, \text{ncracks}$ are the corresponding step functions. Upon finite element discretisation, nodal enrichment with fields \bar{b}_i and $\bar{\bar{b}}_i$ is only needed in elements crossed by crack i .

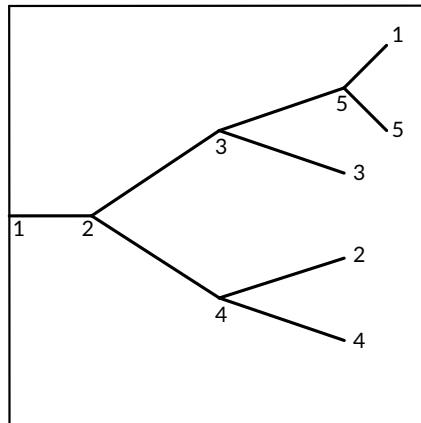


FIGURE 5 Complex pattern with several cracks ($\text{ncracks} = 5$). The numbers indicate the two endpoints of each crack.

2.3 | Crack-fluid pressure

2.3.1 | Simple physical model of a pressurised crack

As discussed in the introduction, the explicit representation of cracks provided by continuous-discontinuous models is an attractive feature in a number of applications. To illustrate this point, we analyse here the effect of a pressurised fluid inside the crack [50].

Consider a domain Ω with boundary $\partial\Omega = \Gamma_u \cup \Gamma_t$ and a crack Γ filled with a fluid at pressure p , see figure

6(a). To keep the discussion simple and focus on the treatment of the pressure and the handling of a discontinuous displacement field in the variational formulation, a local linear elastic bulk is assumed. Regarding continuity, it is convenient to consider also the cracked domain Ω_{cracked} with boundary $\partial\Omega_{\text{cracked}} = \Gamma_u \cup \Gamma_t \cup \Gamma^+ \cup \Gamma^-$, where Γ^+ and Γ^- are the two faces of crack Γ , see figure 6(b). The governing equations are then

$$\nabla \cdot \boldsymbol{\sigma} = \mathbf{0} \text{ in } \Omega_{\text{cracked}} \tag{6a}$$

$$\mathbf{u} = \mathbf{u}^* \text{ on } \Gamma_u \tag{6b}$$

$$\boldsymbol{\sigma} \cdot \mathbf{n} = \mathbf{t}^* \text{ on } \Gamma_t \tag{6c}$$

$$\boldsymbol{\sigma} \cdot \mathbf{n} = -p \mathbf{n} \text{ on } \Gamma^+ \cup \Gamma^- \tag{6d}$$

In addition to the usual equations (6a)-(6c), already shown in table 1, equation (6d) is the pressure boundary condition. Note that the fluid exerts pressure p on both faces of the crack. In this simple physical model, pressure is assumed to be an input. A possible alternative would be to use a poro-mechanical model [51] that couples bulk mechanical deformation and fluid flow, where pressure is an additional unknown field.

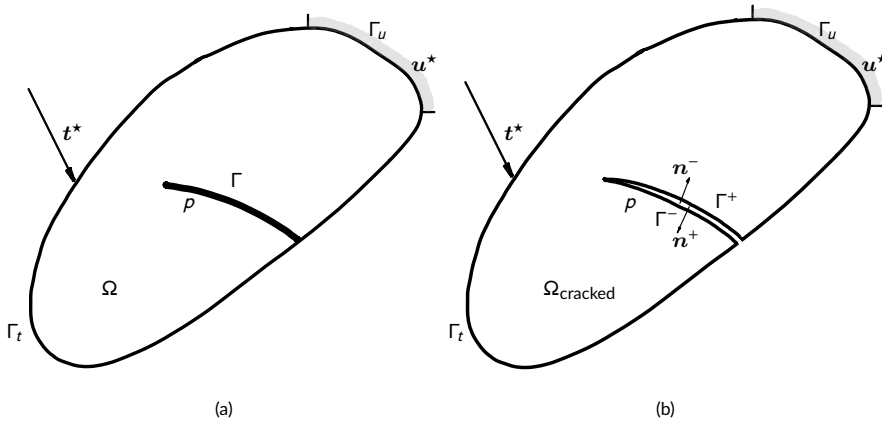


FIGURE 6 Fluid-pressurised crack: (a) domain Ω with crack Γ ; (b) domain Ω_{cracked} with the two faces of the crack, Γ^+ and Γ^- , and the corresponding unit normals, \mathbf{n}^+ and \mathbf{n}^- .

2.3.2 | Variational formulation

The derivation of the weak form of problem (6) follows the standard procedure, because displacements and weight functions are *continuous* in Ω_{cracked} (albeit discontinuous in Ω across Γ). Weighted residuals, integration by parts and Gauss divergence theorem lead to the weak form

“Find \mathbf{u} in Ω_{cracked} such that $\mathbf{u}|_{\Gamma_u} = \mathbf{u}^*$ and

$$\int_{\Omega_{\text{cracked}}} \nabla^s \boldsymbol{\omega} : \boldsymbol{\sigma} d\Omega = \int_{\Gamma_t} \boldsymbol{\omega} \cdot \mathbf{t}^* d\Gamma + \int_{\Gamma^+} \boldsymbol{\omega} \cdot (-p \mathbf{n}^+) d\Gamma + \int_{\Gamma^-} \boldsymbol{\omega} \cdot (-p \mathbf{n}^-) d\Gamma \tag{7}$$

for any $\boldsymbol{\omega}$ in Ω_{cracked} such that $\boldsymbol{\omega}|_{\Gamma_u} = \mathbf{0}$ ". The last two terms in equation (7) represent the external virtual work of the pressure forces.

If a fitted mesh is used, then the finite element discretisation of equation (7) is standard. If, on the other hand, the crack Γ is not meshed but handled by means of X-FEM, then it is convenient to rewrite the weak form (7) as an integral equation over domain Ω . We consider a discontinuous displacement field $\boldsymbol{u}(\boldsymbol{x}) = \boldsymbol{\alpha}(\boldsymbol{x}) + \psi(\boldsymbol{x})\boldsymbol{b}(\boldsymbol{x})$ with $\boldsymbol{\alpha}|_{\Gamma_u} = \boldsymbol{u}^*$ and $\boldsymbol{b}|_{\Gamma_u} = \mathbf{0}$, see equation (2a), and arbitrary test functions $\boldsymbol{\omega}(\boldsymbol{x}) = \boldsymbol{\omega}_a(\boldsymbol{x}) + \psi(\boldsymbol{x})\boldsymbol{\omega}_b(\boldsymbol{x})$ with $\boldsymbol{\omega}_a|_{\Gamma_u} = \boldsymbol{\omega}_b|_{\Gamma_u} = \mathbf{0}$. Substituting $\boldsymbol{\omega}$ in equation (7) and taking into account that *i*) both contributions $\boldsymbol{\omega}_a$ and $\boldsymbol{\omega}_b$ are arbitrary, *ii*) the two normals are opposite vectors, $\boldsymbol{n}^- = -\boldsymbol{n}^+$ and *iii*) $\psi|_{\Gamma^+} = +1$ and $\psi|_{\Gamma^-} = -1$ leads finally to the weak form:

"Find $\boldsymbol{\alpha}$ and \boldsymbol{b} in Ω such that $\boldsymbol{\alpha}|_{\Gamma_u} = \boldsymbol{u}^*$ and $\boldsymbol{b}|_{\Gamma_u} = \mathbf{0}$ and

$$\int_{\Omega} \nabla^s \boldsymbol{\omega}_a : \boldsymbol{\sigma} d\Omega = \int_{\Gamma_t} \boldsymbol{\omega}_a \cdot \boldsymbol{t}^* d\Gamma \quad (8a)$$

$$\int_{\Omega} \psi \nabla^s \boldsymbol{\omega}_b : \boldsymbol{\sigma} d\Omega = \int_{\Gamma_t} \psi \boldsymbol{\omega}_b \cdot \boldsymbol{t}^* d\Gamma + 2 \int_{\Gamma} \boldsymbol{\omega}_b (-p \boldsymbol{n}^+) d\Gamma \quad (8b)$$

for any $\boldsymbol{\omega}_a$ and $\boldsymbol{\omega}_b$ in Ω such that $\boldsymbol{\omega}_a|_{\Gamma_u} = \boldsymbol{\omega}_b|_{\Gamma_u} = \mathbf{0}$."

This weak form clearly reflects the role of crack-fluid pressure. If the virtual displacements are continuous ($\boldsymbol{\omega}_b = \mathbf{0}$), the *net* virtual work of pressure forces is zero, because the contributions on the two crack faces have opposite signs. This is why there is no pressure contribution in equation (8a). If, on the other hand, the virtual displacements are discontinuous across the crack ($\boldsymbol{\omega}_b \neq \mathbf{0}$), then pressure forces open the crack and do a non-zero virtual work, reflected in the last term of equation (8b). Note also the factor 2, associated to the step height of the sign function, $\psi|_{\Gamma^+} - \psi|_{\Gamma^-} = 2$.

2.3.3 | Finite element discretisation

Finite element discretisation of the weak form (8) leads to the linear system of algebraic equations

$$\begin{bmatrix} \mathbf{K}_{aa} & \mathbf{K}_{ab} \\ \mathbf{K}_{ba} & \mathbf{K}_{bb} \end{bmatrix} \begin{Bmatrix} \mathbf{a} \\ \mathbf{b} \end{Bmatrix} = \begin{Bmatrix} \mathbf{f}_a \\ \mathbf{f}_b \end{Bmatrix} \quad (9)$$

where \mathbf{a} is a "long" vector of length ndof (number of standard degrees of freedom) and \mathbf{b} is a "short" vector of length ndof_{Enr} (number of enriched degrees of freedom).

The stiffness matrix and force vector are defined as

$$\mathbf{K}_{aa} = \int_{\Omega} \mathbf{B}_a^T \mathbf{C} \mathbf{B}_a d\Omega \quad \mathbf{K}_{bb} = \int_{\Omega} \mathbf{B}_b^T \mathbf{C} \mathbf{B}_b d\Omega \quad (10a)$$

$$\mathbf{K}_{ab} = \int_{\Omega} \psi \mathbf{B}_a^T \mathbf{C} \mathbf{B}_b d\Omega \quad \mathbf{K}_{ba} = \int_{\Omega} \psi \mathbf{B}_b^T \mathbf{C} \mathbf{B}_a d\Omega \quad (10b)$$

and

$$\mathbf{f}_a = \int_{\Gamma_t} \mathbf{N}_a^T \boldsymbol{t}^* d\Gamma \quad \mathbf{f}_b = \int_{\Gamma_t} \psi \mathbf{N}_b^T \boldsymbol{t}^* d\Gamma + 2 \int_{\Gamma} \psi \mathbf{N}_b^T (-p \boldsymbol{n}^+) d\Gamma \quad (11)$$

where \mathbf{N}_a and \mathbf{B}_a are the usual matrices of shape functions and shape function derivatives, and \mathbf{N}_b and \mathbf{B}_b are the corresponding matrices for enriched degrees of freedom. Since ndof_{Enr} is typically much less than ndof , the compu-

tational burden of the X-FEM enrichment is moderate.

Note in equation (11)₂ the contribution of crack-fluid pressure in vector \mathbf{f}_b . The line integral over crack Γ is computed by mapping, for each cracked element, the corresponding segment to the reference $[-1, 1]$ segment, where a standard Gaussian quadrature is applied.

3 | NUMERICAL EXAMPLES

Two types of numerical examples are shown here. Section 3.1 deals with cracks in a local elastic bulk. The crack geometry is known in advance and non-local displacements are not used; the focus is on X-FEM enrichment for crack branching and on crack opening due to internal pressure. Section 3.2 deals with damage-driven crack branching. All the ingredients in the proposed approach are combined: the gradient-enhanced continuous damage model, the geometrical crack tracking based on the medial axis and the X-FEM discontinuous enrichment.

3.1 | Cracks in an elastic bulk

3.1.1 | Kinematics of one branching element

As a first example, we explore the kinematics of one quadrilateral finite element with a branching crack. As shown in figure 7, the vertical “trunk” and the left branch are regarded as crack Γ_1 and the right branch is crack Γ_2 . The definition of sign functions $\psi_1(x)$ and $\psi_2(x)$ is also shown.

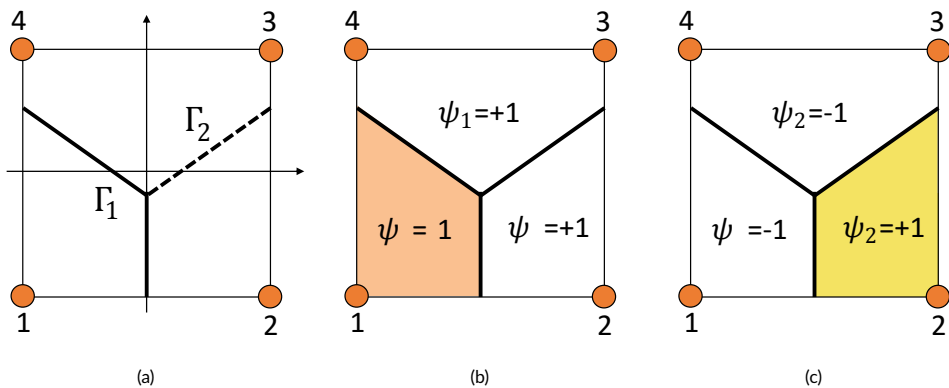


FIGURE 7 One finite element with a branching crack: (a) cracks Γ_1 and Γ_2 ; (b) sign function ψ_1 for crack Γ_1 ; (c) sign function ψ_2 for crack Γ_2 .

All four nodes are enriched with degrees of freedom \mathbf{b}_1 and \mathbf{b}_2 , in addition to the standard degrees of freedom \mathbf{a} , see equation (4). This means that the dimension of the elastic stiffness matrix is 24 ($n_{sd} \times n_{nodes} \times n_{fields}$, with $n_{sd} = 2$, $n_{nodes} = 4$ and $n_{fields} = 3$).

A good test to validate the X-FEM enrichment for this branching element is to compute and plot the rigid eigenmodes of the elastic stiffness matrix (by means of command `eig` in Matlab). Figure 8 shows the expected result: two rigid translations and one rigid rotation for each of the three pieces (that is, a total of nine rigid modes). This clearly

shows that the X-FEM enrichment effectively cuts the finite element into three fully independent pieces, with no spurious stress transmission between them. This full separation does not occur if the branching element is only enriched with weak discontinuities [36].

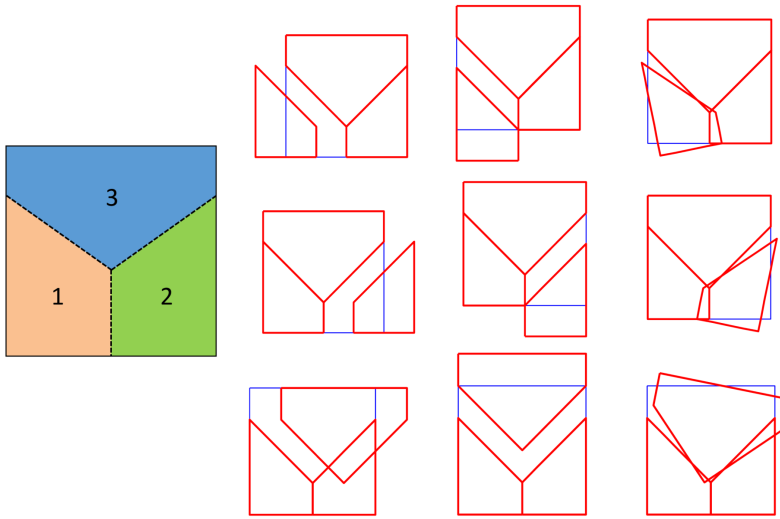


FIGURE 8 Rigid modes in a crack-branching element.

3.1.2 | Fluid pressure on a crack system

We study next the effect of fluid pressure on a crack system, see figure 9. The rectangular domain has length $L = 10$ m, height $H = 7$ m, Young's modulus $E = 20$ GPa and Poisson's coefficient $\nu = 0$. Displacements are restrained in the left and right edges.

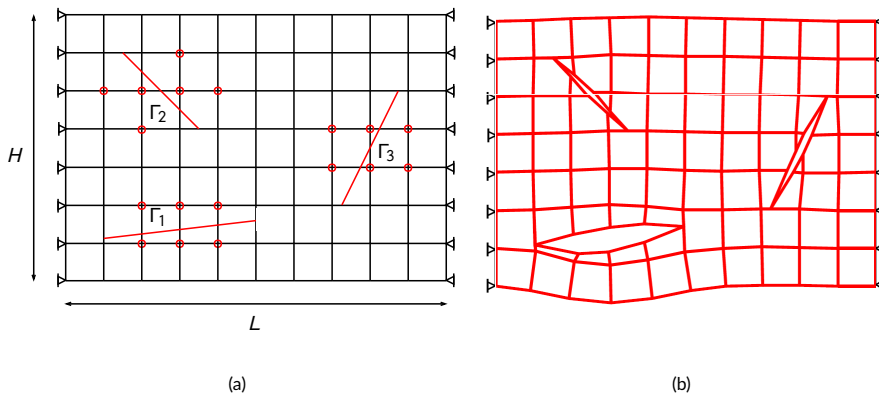


FIGURE 9 Fluid pressure on a crack system: (a) problem statement; (b) deformed mesh (amplification factor: 20).

The domain contains three independent, non-connected cracks Γ_1, Γ_2 and Γ_3 . Nodes enriched with the corresponding sign function ψ_i ($i = 1, 2, 3$) are shown in red. Note that crack tips are assumed to be located in element edges, and that the two nodes in each crack-tip edge are not enriched, because the displacement field is not discontinuous along them.

Cracks are filled with a fluid with pressure $p = 0.05$ GPa. This leads to nodal forces in the enriched nodes, computed according to equation (11)₂. The resulting deformed mesh is plotted in figure 9(b). Note how the crack opening is larger in Γ_1 , which is less confined by the boundary conditions, than in the other two cracks.

In this simple scenario of a pre-existing and non-evolving crack system, the dimension of the linear system (9) is fixed, with $\text{ndof}=176$ and $\text{ndofEnr}=36$. It can be checked that the X-FEM enrichment has a moderate impact on the conditioning of the stiffness matrix. The 2-norm condition number (command `cond` in Matlab) of the stiffness matrix of the bulk without cracks (i.e. matrix \mathbf{K}_{aa} in equation (10), with restrained displacements imposed by means of Lagrange multipliers, see [50]) is 2.2×10^3 , whereas for the cracked bulk (that is, accounting also for blocks \mathbf{K}_{ab} , \mathbf{K}_{ba} and \mathbf{K}_{bb}) it is 3.0×10^3 .

3.1.3 | Recursive crack branching

In this example we illustrate that the X-FEM enrichment of the displacement field can be applied recursively to an arbitrary number of cracks, see equation (5a), by means of a simple test.

Consider the rectangular specimen of dimensions $60 \text{ mm} \times 100 \text{ mm}$ and elastic parameters $E = 20$ GPa and $\nu = 0$ shown in figure 10. We assume that a pressurised fluid with $p = 0.05$ GPa causes the evolving crack system shown in figures 10(a)-10(d) and compute the corresponding crack opening patterns, shown in figures 10(f)-10(j). The boundary conditions and the finite element mesh are shown in figure 10(e).

These opening patterns are obtained by means of the X-FEM enrichment of the displacement field in equation (5a). The variable `ncracks` increases progressively from 1 to 4. Note how the complete crack system composed of cracks $\Gamma_1, \Gamma_2, \Gamma_3$ and Γ_4 finally fracture the medium into five fully independent pieces, with no spurious stress transmission between them.

Table 2 reflects the evolving nature of the crack system. The length of nodal vector \mathbf{a} (that is, `ndof`) is constant throughout the process, whereas the number `ncracks` and length `ndofEnr i` of vectors \mathbf{b}_i (with $i = 1, \dots, 4$) increase as the cracks branch and propagate. There is also a noticeable but modest increase in the condition number of the global stiffness matrix.

TABLE 2 Recursive crack branching: evolution of vector dimensions and problem conditioning

Phase	<code>ncracks</code>	<code>ndof</code>	<code>ndofEnr1</code>	<code>ndofEnr2</code>	<code>ndofEnr3</code>	<code>ndofEnr4</code>	Condition number
1	1	48	4	—	—	—	35.6
2	2	48	8	4	—	—	588
3	2	48	12	8	—	—	735
4	4	48	20	16	8	8	883
5	4	48	24	20	12	12	1400

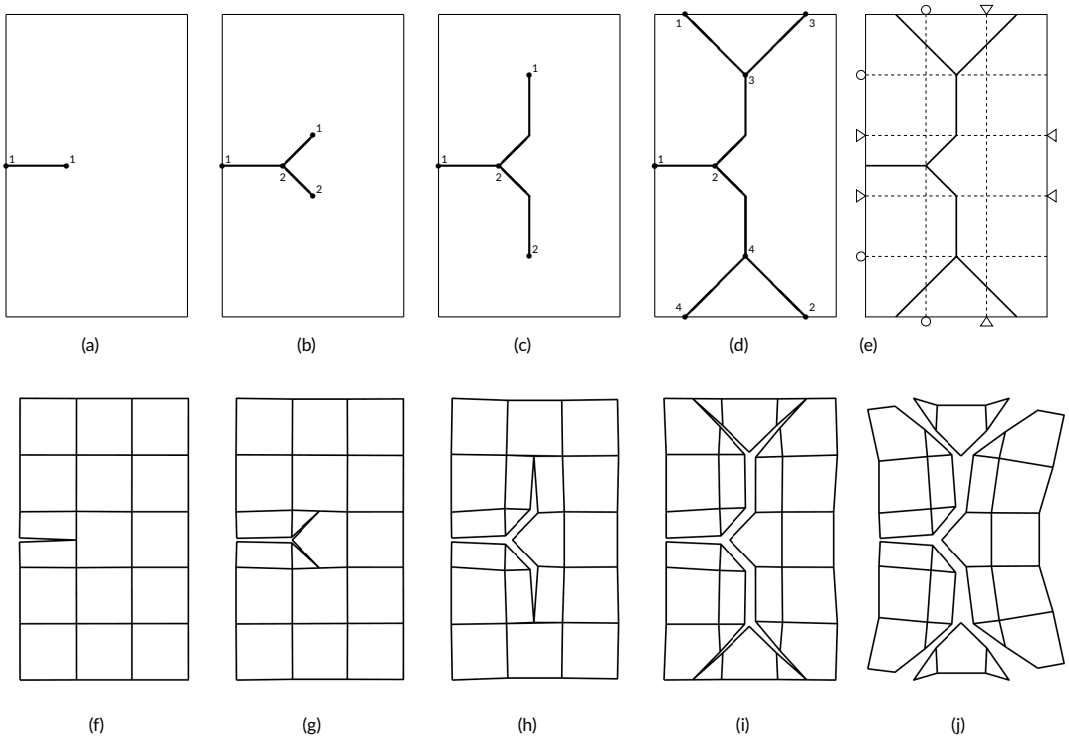


FIGURE 10 Recursive crack branching: (a-d) evolution of the crack geometry, with the endpoints of each crack indicated by numbers; (e) ; (f-i) evolution of the crack opening (amplification factor: 20).

3.2 | Damage-driven crack branching

The square specimen of figure 11 is clamped at the right edge and subjected to triangular distributions of prescribed displacements at the top and bottom edges. The bulk is modelled as an elastic-damage material, with the Mazars definition of the equivalent strain (based on positive principal strains) and a linear softening law (with damage-initiation strain κ_i and ultimate strain κ_u [2]). The domain is meshed with a regular grid of 31×31 linear quadrilateral finite elements. Mode I damage inception at the centre of the left edge is triggered by a notch of 3×1 finite elements. Table 3 summarises the geometrical and material parameters.

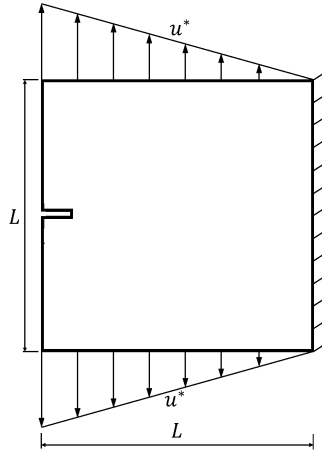


FIGURE 11 Damage-driven branching: problem statement

TABLE 3 Damage-driven branching: geometrical and material parameters

Meaning	Symbol	Value
Size of the specimen	L	100 mm
Length of notch	L_W	$3L/101$
Height of notch	h_W	$L/101$
Young's modulus	E	20 000 MPa
Young's modulus of weaker part	E_W	2 000 MPa
Poisson's coefficient	ν	0.3
Damage initiation strain	κ_i	10^{-4}
Ultimate strain	κ_u	1.25×10^{-2}
Characteristic length	ℓ	$\sqrt{7} \times 10^{-1}$ mm

Figure 12(a)-(c) shows the evolution of the damage field D in the continuous regime for increasing values of the

prescribed displacement u^* . As expected, damage starts at the notch and propagates rightward up to a point where it becomes energetically more efficient to bifurcate into two symmetrical branches. There are no heterogeneities in this problem; the boundary conditions are responsible for branching.

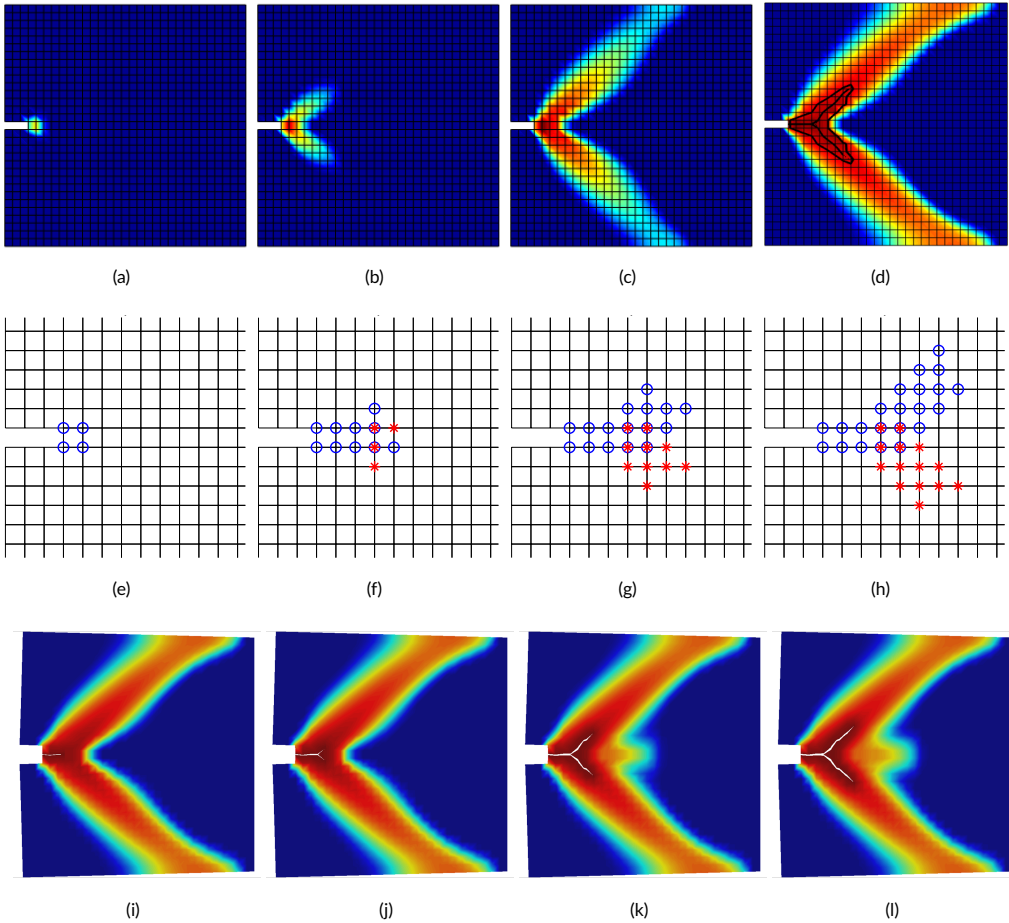


FIGURE 12 Damage-driven branching: (a)-(c) evolution of the damage field in the continuous regime; (d) isoline and medial axis at the transition point; (e)-(h) progressive X-FEM enrichment of nodes for crack Γ_1 (blue circles) and crack Γ_2 (red crosses); (i)-(l) evolution of the damage field and opening of the sharp crack in the discontinuous regime (amplification factor: 100).

When damage reaches the critical value $D_{\text{crit}} = 0.995$ in the most damaged element, the model switches to the continuous-discontinuous regime. Figure 12(d) shows the damage isoline $D = D^* = 0.9$ and its θ -simplified medial axis, with a separation angle $\theta = 100^\circ$, see section 2.2.1. We stress the fact that the medial axis automatically captures the branching of the damage field, without resorting to any ad-hoc branching criterion, and leads to a branching sharp crack. Note also that the medial axis is rather insensitive to the values of both the separation angle and the damage isoline D^* [2].

The nodes in the elements crossed by the medial axis are progressively enriched as the crack propagates when

D reaches D_{crit} , see figure 12(e)-(h). The X-FEM enrichment of the displacement field is carried out as discussed in section 2.2.2. Note that the four nodes of the branching finite element are enriched with both \mathbf{b}_1 and \mathbf{b}_2 degrees of freedom.

Hence, the complete modelling approach consists in applying the three main steps outlined above –that is, the computation of the damage field, the determination of the medial axis, and the X-FEM enrichment– within the usual load stepping in nonlinear analysis. As the damage field expands, so does the damage isoline $D = D^*$ and its medial axis. This results in a sharp crack that starts propagating rightward and then branches, see figure 12(i)-(l). Note how, in this continuous-discontinuous approach, the background damage field governs in a natural manner the propagation and branching of the crack.

Figure 13 shows the force-displacement response obtained with the proposed continuous-discontinuous approach. For comparison purposes, the response of the continuous approach (i.e. no X-FEM enrichment of the displacement field) is also shown. The two curves are rather different after the transition point: in the continuous-discontinuous approach, the insertion of a *traction-free* sharp crack results in a loss of load-carrying capacity. One possible remedy would be to replace the traction-free crack by an energetically equivalent cohesive crack; work in this direction is under progress. Energetic non-equivalence between the continuous and the continuous-discontinuous approaches may also be the cause of the growth of damage along the middle line that can be seen in figure 12(k)-(l).

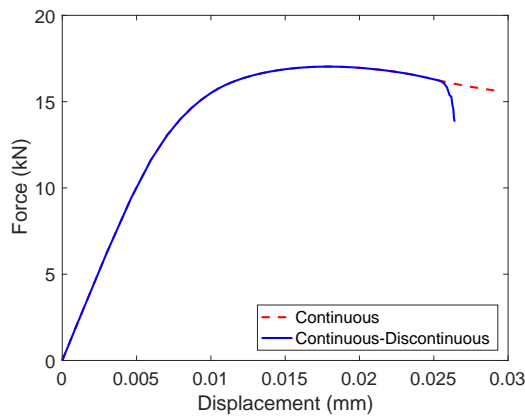


FIGURE 13 Force-displacement curves for the continuous and continuous-discontinuous approaches.

4 | CONCLUDING REMARKS

A new continuous-discontinuous formulation for fracture that accounts for crack branching in a natural manner is presented. Its key ingredients are *i)* a displacement-based nonlocal continuum damage model for diffuse cracks, *ii)* a global geometrical crack tracking technique based on the medial-axis concept, and *iii)* the X-FEM enrichment of the displacement field for sharp cracks. The capability of the model to capture branching cracks without any ad-hoc branching criteria originates from the generality of the medial axis, which detects the bifurcation in the damage field. This generality opens the door to the extension of the model to three dimensions, where the notion of medial axis is replaced by that of medial surface. This idea has already been tested for simple, planar (i.e. non-branching) cracks

[1, 2].

The proposed model also includes a crack-fluid pressure. In this work, it is regarded as an input. However, the model could be further extended to add hydrodynamics, thus resulting in a coupled fluid-structure problem, with pressure as an additional unknown. Another possible improvement of the model is the replacement of traction-free sharp cracks by energetically equivalent cohesive cracks. This has also already been tested for non-branching cracks [8].

Finally, we note that, since the goal of this contribution is presenting the model and illustrating its possibilities for dealing with crack branching and crack pressure, uniform linear finite element meshes have been used in all the numerical examples. Some sort of adaptivity should be used to increase the computational efficiency, especially in 3D problems.

Acknowledgments

The first author publishes with the permission of the Executive Director of the British Geological Survey.

references

- [1] Tamayo-Mas E. Continuous-discontinuous modelling for quasi-brittle failure: propagating cracks in a regularised bulk. PhD thesis, Universitat Politècnica de Catalunya; 2013.
- [2] Tamayo-Mas E, Rodríguez-Ferran A. A medial-axis-based model for propagating cracks in a regularised bulk. *International Journal for Numerical Methods in Engineering* 2015;101(7):489–520.
- [3] Pijaudier-Cabot G, Bažant Z. Nonlocal Damage Theory. *Journal of Engineering Mechanics* 1987;113(10):1512–1533.
- [4] Peerlings R, de Borst R, Brekelmans W, Geers M. Gradient-enhanced damage modelling of concrete fracture. *Mechanics of Cohesive-frictional Materials* 1998;3(4):323–342.
- [5] Bourdin B, Francfort G, Marigo JJ. Numerical experiments in revisited brittle fracture. *Journal of the Mechanics and Physics of Solids* 2000;48(4):797–826.
- [6] Ambati M, Gerasimov T, De Lorenzis L. A review on phase-field models of brittle fracture and a new fast hybrid formulation. *Computational Mechanics* 2015;55(2):383–405.
- [7] Comi C, Mariani S, Perego U. An extended FE strategy for transition from continuum damage to mode I cohesive crack propagation. *International Journal for Numerical and Analytical Methods in Geomechanics* 2007;31(2):213–238.
- [8] Tamayo-Mas E, Rodríguez-Ferran A. A new continuous-discontinuous damage model: Cohesive cracks via an accurate energy-transfer process. *Theoretical and Applied Fracture Mechanics* 2014;69:90–101.
- [9] Wang Y, Waisman H. From diffuse damage to sharp cohesive cracks: A coupled XFEM framework for failure analysis of quasi-brittle materials. *Computer Methods in Applied Mechanics and Engineering* 2016;299:57–89.
- [10] Roth SN, Léger P, Soulaïmani A. A combined XFEM-damage mechanics approach for concrete crack propagation. *Computer Methods in Applied Mechanics and Engineering* 2015;283:923–955.
- [11] Lé B, Moës N, Legrain G. Coupling damage and cohesive zone models with the Thick Level Set approach to fracture. *Engineering Fracture Mechanics* 2018;193:214–247.
- [12] Geelen R, Liu Y, Dolbow J, Rodríguez-Ferran A. An optimization-based phase-field approach for continuous-discontinuous crack propagation. *International Journal for Numerical Methods in Engineering* 2018;116(1):1–20.

- [13] Jirásek M, Zimmermann T. Embedded crack model. Part II: combination with smeared cracks. *International Journal for Numerical Methods in Engineering* 2001;50(6):1291–1305.
- [14] Simone A, Wells G, Sluys L. From continuous to discontinuous failure in a gradient-enhanced continuum damage model. *Computer Methods in Applied Mechanics and Engineering* 2003;192(41-42):4581–4607.
- [15] Giovanardi B, Scotti A, Formaggia L. A hybrid XFEM-Phase field (*Xfield*) method for crack propagation in brittle elastic materials. *Computer Methods in Applied Mechanics and Engineering* 2017;320:396–420.
- [16] Belytschko T, Black T. Elastic crack growth in finite elements with minimal remeshing. *International Journal for Numerical Methods in Engineering* 1999;45(5):601–620.
- [17] Moës N, Dolbow J, Belytschko T. A finite element method for crack growth without remeshing. *International Journal for Numerical Methods in Engineering* 1999;46(1):131–150.
- [18] Simo J, Oliver J, Armero F. An analysis of strong discontinuities induced by strain-softening in rate-independent inelastic solids. *Computational Mechanics* 1993;12(5):277–296.
- [19] Mazars J, Pijaudier-Cabot G. From damage to fracture mechanics and conversely: A combined approach. *International Journal of Solids and Structures* 1996;33(20-22):3327–3342.
- [20] Wells G, Sluys L, de Borst R. Simulating the propagation of displacement discontinuities in a regularized strain-softening medium. *International Journal for Numerical Methods in Engineering* 2002;53(5):1235–1256.
- [21] Seabra M, César de Sá J, Andrade F, Pires F. Continuous-discontinuous formulation for ductile fracture. *International Journal of Material Forming* 2011;4(3):271–281.
- [22] Cazes F, Coret M, Combescure A, Gravouil A. A thermodynamic method for the construction of a cohesive law from a nonlocal damage model. *International Journal of Solids and Structures* 2009;46(6):1476–1490.
- [23] Cazes F, Simatos A, Coret M, Combescure A. A cohesive zone model which is energetically equivalent to a gradient-enhanced coupled damage-plasticity model. *European Journal of Mechanics - A/Solids* 2010;29(6):976–989.
- [24] Cuvilliez S, Feyel F, Lorentz E, Michel-Ponnelle S. A finite element approach coupling a continuous gradient damage model and a cohesive zone model within the framework of quasi-brittle failure. *Computer Methods in Applied Mechanics and Engineering* 2012;237-240(0):244–259.
- [25] Benvenuti E, Tralli A. Simulation of finite-width process zone in concrete-like materials by means of a regularized extended finite element model. *Computational Mechanics* 2012;50(4):479–497.
- [26] Giry C, Dufour F, Mazars J. Stress-based nonlocal damage model. *International Journal of Solids and Structures* 2011;48(25-26):3431–3443.
- [27] Bobiński J, Tejchman J. A coupled constitutive model for fracture in plain concrete based on continuum theory with non-local softening and eXtended Finite Element Method. *Finite Elements in Analysis and Design* 2016;114:1–21.
- [28] Moës N, Stolz C, Bernard P, Chevaugeon N. A level set based model for damage growth: The thick level set approach. *International Journal for Numerical Methods in Engineering* 2011;86(3):358–380.
- [29] Wu C, Ma N, Takada K, Okada H. A meshfree continuous-discontinuous approach for the ductile fracture modeling in explicit dynamics analysis. *Computational Mechanics* 2016;58(3):391–409.
- [30] Huerta A, Belytschko T, Fernández-Méndez S, Rabczuk T, Zhuang X, Arroyo M. Meshfree Methods. In: Stein E, de Borst R, Hughes T, editors. *Encyclopedia of Computational Mechanics Second Edition, Part 2 Fundamentals* Chichester: Wiley; 2017.

- [31] Wang Y, Zhou X, Wang Y, Shou Y. A 3-D conjugated bond-pair-based peridynamic formulation for initiation and propagation of cracks in brittle solids. *International Journal of Solids and Structures* 2018;134:89–115.
- [32] Zaccariotto M, Mudric T, Tomasi D, Shojaei A, Galvanetto U. Coupling of FEM meshes with Peridynamic grids. *Computer Methods in Applied Mechanics and Engineering* 2018;330:471–497.
- [33] Freund L. *Dynamic fracture mechanics*. Cambridge University Press; 1998.
- [34] Bleyer J, Roux-Langlois C, Molinari JF. Dynamic crack propagation with a variational phase-field model: limiting speed, crack branching and velocity-toughening mechanisms. *International Journal of Fracture* 2017;204(1):79–100.
- [35] Linder C, Armero F. Finite elements with embedded branching. *Finite Elements in Analysis and Design* 2009;45(4):280–293.
- [36] Lloberas-Valls O, Huespe A, Oliver J, Dias I. Strain injection techniques in dynamic fracture modeling. *Computer Methods in Applied Mechanics and Engineering* 2016;308:499–534.
- [37] Wu T, Carpiuc-Prisacari A, Poncelet M, De Lorenzis L. Phase-field simulation of interactive mixed-mode fracture tests on cement mortar with full-field displacement boundary conditions. *Engineering Fracture Mechanics* 2017;182:658–688.
- [38] Hofacker M, Miehe C. A phase field model of dynamic fracture: Robust field updates for the analysis of complex crack patterns. *International Journal for Numerical Methods in Engineering* 2013;93(3):276–301.
- [39] Arias I, Knap J, Chalivendra V, Hong S, Michael O, Rosakis A. Numerical modelling and experimental validation of dynamic fracture events along weak planes. *Computer Methods in Applied Mechanics and Engineering* 2007;196(37-40):3833–3840.
- [40] Daux C, Moës N, Dolbow J, Sukumar N, Belytschko T. Arbitrary branched and intersecting cracks with the extended finite element method. *International Journal for Numerical Methods in Engineering* 2000;48(12):1741–1760.
- [41] Richardson C, Hegemann J, Sifakis E, Hellrung J, Teran J. An XFEM method for modeling geometrically elaborate crack propagation in brittle materials. *International Journal for Numerical Methods in Engineering* 2011;88(10):1042–1065.
- [42] Rodríguez-Ferran A, Morata I, Huerta A. Efficient and reliable nonlocal damage models. *Computer Methods in Applied Mechanics and Engineering* 2004;193(30-32):3431–3455.
- [43] Rodríguez-Ferran A, Morata I, Huerta A. A new damage model based on non-local displacements. *International Journal for Numerical and Analytical Methods in Geomechanics* 2005;29(5):473–493.
- [44] Mestre-Bellido H. *Damage initiation and propagation in non-local gradient models based on displacement smoothing*. MSc thesis, Universitat Politècnica de Catalunya; 2016.
- [45] Suresh K, 2D Medial Axis Computation; 2006. Accessed on 14 September 2018. <http://www.mathworks.com/matlabcentral/fileexchange/12399-2-d-medial-axis-computation>.
- [46] Yoshizawa S, SM03 Skeleton; 2008. Accessed on 14 September 2018. <http://www.riken.jp/briect/Yoshizawa/Research/Skeleton.html>.
- [47] Ziaei-Rad V, Shen L, Jiang J, Shen Y. Identifying the crack path for the phase field approach to fracture with non-maximum suppression. *Computer Methods in Applied Mechanics and Engineering* 2016;312:304–321.
- [48] Feliu-Fabà J. *A continuous-discontinuous model to simulate crack branching in quasi-brittle failure*. MSc thesis, Universitat Politècnica de Catalunya; 2016.
- [49] Foskey M, Lin M, Manocha D. Efficient computation of a simplified medial axis. In: *Proceedings of the eighth ACM symposium on Solid modeling and applications SM '03*, New York, NY, USA: ACM; 2003. p. 96–107. <http://doi.acm.org/10.1145/781606.781623>.

-
- [50] Casado-Antolin M. A continuous-discontinuous model to introduce fluid pressure in a crack. BSc thesis, Universitat Politècnica de Catalunya; 2016.
 - [51] Prévost JH, Sukumar N. Faults simulations for three-dimensional reservoir-geomechanical models with the extended finite element method. *Journal of the Mechanics and Physics of Solids* 2016;86:1–18.
 - [52] Ventura G, Benvenuti E. Equivalent polynomials for quadrature in Heaviside function enriched elements. *International Journal for Numerical Methods in Engineering* 2015;102(3-4):688–710.

A | VARIATIONAL FORMULATION AND CONSISTENT LINEARISATION

In this appendix, the variational formulation and the consistent tangent matrix of the proposed model are derived [48]. Particular emphasis is placed on the terms that are required to describe branching cracks, which were not included in previous formulations [1, 2].

A.1 | Variational formulation

Consider a domain Ω with boundary $\partial\Omega = \Gamma_u \cup \Gamma_t$ and a branching crack $\Gamma = \Gamma_1 \cup \Gamma_2$, see figure 6(a). As discussed in section 2.3.2, it is convenient to state the problem in the cracked domain Ω_{cracked} , with boundary $\partial\Omega_{\text{cracked}} = \Gamma_u \cup \Gamma_t \cup \Gamma_1^+ \cup \Gamma_1^- \cup \Gamma_2^+ \cup \Gamma_2^-$, see figure 6(b). The coupled problem (equilibrium equation and regularisation equation) in Ω_{cracked} reads

$$\nabla \cdot \boldsymbol{\sigma}(\mathbf{u}, \tilde{\mathbf{u}}) = \mathbf{0} \text{ in } \Omega_{\text{cracked}} \quad (12a)$$

$$\mathbf{u} = \mathbf{u}^* \text{ on } \Gamma_u \quad (12b)$$

$$\boldsymbol{\sigma} \cdot \mathbf{n} = \mathbf{t}^* \text{ on } \Gamma_t \quad (12c)$$

$$\boldsymbol{\sigma} \cdot \mathbf{n} = -\rho \mathbf{n} \text{ on } \Gamma_1^+ \cup \Gamma_1^- \cup \Gamma_2^+ \cup \Gamma_2^- \quad (12d)$$

$$\tilde{\mathbf{u}} - \ell^2 \nabla^2 \tilde{\mathbf{u}} = \mathbf{u} \text{ in } \Omega_{\text{cracked}} \quad (12e)$$

$$\tilde{\mathbf{u}} \cdot \mathbf{n} = \mathbf{u} \cdot \mathbf{n} \text{ in } \partial\Omega_{\text{cracked}} \quad (12f)$$

$$\mathbf{n} \cdot \nabla \tilde{\mathbf{u}} \cdot \boldsymbol{\tau} = \mathbf{n} \cdot \nabla \mathbf{u} \cdot \boldsymbol{\tau} \text{ in } \partial\Omega_{\text{cracked}} \quad (12g)$$

Equations (12) are essentially the same as equations (1), but with the addition of the pressure boundary condition (12d) on the two faces of the two cracks.

The weak form of problem (12) is obtained following standard procedures, because fields \mathbf{u} (local displacements), $\tilde{\mathbf{u}}$ (non-local displacements), $\boldsymbol{\omega}$ (test functions for equilibrium equation) and $\tilde{\boldsymbol{\omega}}$ (test functions for regularisation equation) are continuous in the cracked domain Ω_{cracked} . It reads

“Find \mathbf{u} and $\tilde{\mathbf{u}}$ in Ω_{cracked} such that $\mathbf{u} = \mathbf{u}^*$ on Γ_u , $\tilde{\mathbf{u}} \cdot \mathbf{n} = \mathbf{u} \cdot \mathbf{n}$ on $\partial\Omega_{\text{cracked}}$ and

$$\int_{\Omega_{\text{cracked}}} \nabla^s \boldsymbol{\omega} : \boldsymbol{\sigma}(\mathbf{u}, \tilde{\mathbf{u}}) \, d\Omega = \int_{\Gamma_t} \boldsymbol{\omega} \cdot \mathbf{t}^* \, d\Gamma + \int_{\Gamma_1^+} \boldsymbol{\omega} \cdot (-\rho \mathbf{n}^+) \, d\Gamma + \int_{\Gamma_1^-} \boldsymbol{\omega} \cdot (-\rho \mathbf{n}^-) \, d\Gamma + \int_{\Gamma_2^+} \boldsymbol{\omega} \cdot (-\rho \mathbf{n}^+) \, d\Gamma + \int_{\Gamma_2^-} \boldsymbol{\omega} \cdot (-\rho \mathbf{n}^-) \, d\Gamma \quad (13a)$$

$$\int_{\Omega_{\text{cracked}}} \tilde{\boldsymbol{\omega}} \cdot \tilde{\mathbf{u}} \, d\Omega + \ell^2 \int_{\Omega_{\text{cracked}}} \nabla \tilde{\boldsymbol{\omega}} : \nabla \tilde{\mathbf{u}} \, d\Omega = \int_{\Omega_{\text{cracked}}} \tilde{\boldsymbol{\omega}} \cdot \mathbf{u} \, d\Omega + \ell^2 \int_{\partial\Omega_{\text{cracked}}} (\tilde{\boldsymbol{\omega}} \cdot \boldsymbol{\tau})(\mathbf{n} \cdot \nabla \mathbf{u} \cdot \boldsymbol{\tau}) \, d\Gamma \quad (13b)$$

for any $\boldsymbol{\omega}$ and $\tilde{\boldsymbol{\omega}}$ in Ω_{cracked} such that $\boldsymbol{\omega} = \mathbf{0}$ on Γ_u and $\tilde{\boldsymbol{\omega}} \cdot \mathbf{n} = \mathbf{0}$ on $\partial\Omega_{\text{cracked}}$.”

We now rewrite the weak form (13) over domain Ω with cracks Γ_1 and Γ_2 . To do so, we consider discontinuous

fields in Ω ,

$$\mathbf{u}(\mathbf{x}) = \mathbf{a}(\mathbf{x}) + \psi_1(\mathbf{x})\mathbf{b}_1(\mathbf{x}) + \psi_2(\mathbf{x})\mathbf{b}_2(\mathbf{x}) \quad (14a)$$

$$\tilde{\mathbf{u}}(\mathbf{x}) = \tilde{\mathbf{a}}(\mathbf{x}) + \psi_1(\mathbf{x})\tilde{\mathbf{b}}_1(\mathbf{x}) + \psi_2(\mathbf{x})\tilde{\mathbf{b}}_2(\mathbf{x}) \quad (14b)$$

$$\boldsymbol{\omega}(\mathbf{x}) = \boldsymbol{\omega}_a(\mathbf{x}) + \psi_1(\mathbf{x})\boldsymbol{\omega}_{b_1}(\mathbf{x}) + \psi_2(\mathbf{x})\boldsymbol{\omega}_{b_2}(\mathbf{x}) \quad (14c)$$

$$\tilde{\boldsymbol{\omega}}(\mathbf{x}) = \tilde{\boldsymbol{\omega}}_a(\mathbf{x}) + \psi_1(\mathbf{x})\tilde{\boldsymbol{\omega}}_{b_1}(\mathbf{x}) + \psi_2(\mathbf{x})\tilde{\boldsymbol{\omega}}_{b_2}(\mathbf{x}) \quad (14d)$$

and replace them in the weak form (13). Taking into account that i) $\boldsymbol{\omega}_a, \boldsymbol{\omega}_{b_1}, \boldsymbol{\omega}_{b_2}, \tilde{\boldsymbol{\omega}}_a, \tilde{\boldsymbol{\omega}}_{b_1}$ and $\tilde{\boldsymbol{\omega}}_{b_2}$ are arbitrary; ii) $\mathbf{n}^- = -\mathbf{n}^+$ in the crack faces and iii) $\psi_i|_{\Gamma_i^+} = +1$ and $\psi_i|_{\Gamma_i^-} = -1$ leads finally to the weak form

“Find $\mathbf{a}, \mathbf{b}_1, \mathbf{b}_2, \tilde{\mathbf{a}}, \tilde{\mathbf{b}}_1, \tilde{\mathbf{b}}_2$ in Ω such that $\mathbf{a} = \mathbf{u}^*$, $\mathbf{b}_1 = \mathbf{b}_2 = \mathbf{0}$ on Γ_u , $\tilde{\mathbf{a}} \cdot \mathbf{n} = \mathbf{a} \cdot \mathbf{n}$, $\tilde{\mathbf{b}}_1 \cdot \mathbf{n} = \mathbf{b}_1 \cdot \mathbf{n}$, $\tilde{\mathbf{b}}_2 \cdot \mathbf{n} = \mathbf{b}_2 \cdot \mathbf{n}$ on $\partial\Omega \cup \Gamma_1 \cup \Gamma_2$ and

$$\int_{\Omega} \nabla^s \boldsymbol{\omega}_a : \boldsymbol{\sigma}(\mathbf{a}, \mathbf{b}_1, \mathbf{b}_2, \tilde{\mathbf{a}}, \tilde{\mathbf{b}}_1, \tilde{\mathbf{b}}_2) d\Omega = \int_{\Gamma_t} \boldsymbol{\omega}_a \cdot \mathbf{t}^* d\Gamma \quad (15a)$$

$$\int_{\Omega} \psi_1 \nabla^s \boldsymbol{\omega}_{b_1} : \boldsymbol{\sigma} d\Omega = \int_{\Gamma_t} \psi_1 \boldsymbol{\omega}_{b_1} \cdot \mathbf{t}^* d\Gamma + 2 \int_{\Gamma_1} \boldsymbol{\omega}_{b_1} \cdot (-\rho \mathbf{n}^+) d\Omega \quad (15b)$$

$$\int_{\Omega} \psi_2 \nabla^s \boldsymbol{\omega}_{b_2} : \boldsymbol{\sigma} d\Omega = \int_{\Gamma_t} \psi_2 \boldsymbol{\omega}_{b_2} \cdot \mathbf{t}^* d\Gamma + 2 \int_{\Gamma_2} \boldsymbol{\omega}_{b_2} \cdot (-\rho \mathbf{n}^+) d\Omega \quad (15c)$$

$$\begin{aligned} & \int_{\Omega} \tilde{\boldsymbol{\omega}}_a \cdot (\tilde{\mathbf{a}} + \psi_1 \tilde{\mathbf{b}}_1 + \psi_2 \tilde{\mathbf{b}}_2) d\Omega + \ell^2 \int_{\Omega} \nabla \tilde{\boldsymbol{\omega}}_a : (\nabla \tilde{\mathbf{a}} + \psi_1 \nabla \tilde{\mathbf{b}}_1 + \psi_2 \nabla \tilde{\mathbf{b}}_2) d\Omega = \\ & \int_{\Omega} \tilde{\boldsymbol{\omega}}_a \cdot (\mathbf{a} + \psi_1 \mathbf{b}_1 + \psi_2 \mathbf{b}_2) d\Omega + \ell^2 \int_{\partial\Omega} (\tilde{\boldsymbol{\omega}}_a \cdot \boldsymbol{\tau}) [\mathbf{n} \cdot (\nabla \mathbf{a} + \psi_1 \nabla \mathbf{b}_1 + \psi_2 \nabla \mathbf{b}_2) \cdot \boldsymbol{\tau}] d\Gamma + \\ & 2\ell^2 \int_{\Gamma_1} (\tilde{\boldsymbol{\omega}}_a \cdot \boldsymbol{\tau})(\mathbf{n}^+ \cdot \nabla \mathbf{b}_1 \cdot \boldsymbol{\tau}) d\Gamma + 2\ell^2 \int_{\Gamma_2} (\tilde{\boldsymbol{\omega}}_a \cdot \boldsymbol{\tau})(\mathbf{n}^+ \cdot \nabla \mathbf{b}_2 \cdot \boldsymbol{\tau}) d\Gamma \end{aligned} \quad (15d)$$

$$\begin{aligned} & \int_{\Omega} \psi_1 \tilde{\boldsymbol{\omega}}_{b_1} \cdot (\tilde{\mathbf{a}} + \psi_1 \tilde{\mathbf{b}}_1 + \psi_2 \tilde{\mathbf{b}}_2) d\Omega + \ell^2 \int_{\Omega} \psi_1 \nabla \tilde{\boldsymbol{\omega}}_{b_1} : (\nabla \tilde{\mathbf{a}} + \psi_1 \nabla \tilde{\mathbf{b}}_1 + \psi_2 \nabla \tilde{\mathbf{b}}_2) d\Omega = \\ & \int_{\Omega} \psi_1 \tilde{\boldsymbol{\omega}}_{b_1} \cdot (\mathbf{a} + \psi_1 \mathbf{b}_1 + \psi_2 \mathbf{b}_2) d\Omega + \ell^2 \int_{\partial\Omega} (\psi_1 \tilde{\boldsymbol{\omega}}_{b_1} \cdot \boldsymbol{\tau}) [\mathbf{n} \cdot (\nabla \mathbf{a} + \psi_1 \nabla \mathbf{b}_1 + \psi_2 \nabla \mathbf{b}_2) \cdot \boldsymbol{\tau}] d\Gamma + \\ & 2\ell^2 \int_{\Gamma_1} (\tilde{\boldsymbol{\omega}}_{b_1} \cdot \boldsymbol{\tau}) [\mathbf{n}^+ \cdot (\nabla \mathbf{a} + \psi_2 \nabla \mathbf{b}_2) \cdot \boldsymbol{\tau}] d\Gamma + 2\ell^2 \int_{\Gamma_2} (\psi_1 \tilde{\boldsymbol{\omega}}_{b_1} \cdot \boldsymbol{\tau})(\mathbf{n}^+ \cdot \nabla \mathbf{b}_2 \cdot \boldsymbol{\tau}) d\Gamma \end{aligned} \quad (15e)$$

$$\begin{aligned} & \int_{\Omega} \psi_2 \tilde{\boldsymbol{\omega}}_{b_2} \cdot (\tilde{\mathbf{a}} + \psi_1 \tilde{\mathbf{b}}_1 + \psi_2 \tilde{\mathbf{b}}_2) d\Omega + \ell^2 \int_{\Omega} \psi_2 \nabla \tilde{\boldsymbol{\omega}}_{b_2} : (\nabla \tilde{\mathbf{a}} + \psi_1 \nabla \tilde{\mathbf{b}}_1 + \psi_2 \nabla \tilde{\mathbf{b}}_2) d\Omega = \\ & \int_{\Omega} \psi_2 \tilde{\boldsymbol{\omega}}_{b_2} \cdot (\mathbf{a} + \psi_1 \mathbf{b}_1 + \psi_2 \mathbf{b}_2) d\Omega + \ell^2 \int_{\partial\Omega} (\psi_2 \tilde{\boldsymbol{\omega}}_{b_2} \cdot \boldsymbol{\tau}) [\mathbf{n} \cdot (\nabla \mathbf{a} + \psi_1 \nabla \mathbf{b}_1 + \psi_2 \nabla \mathbf{b}_2) \cdot \boldsymbol{\tau}] d\Gamma + \\ & 2\ell^2 \int_{\Gamma_1} (\psi_2 \tilde{\boldsymbol{\omega}}_{b_2} \cdot \boldsymbol{\tau})(\mathbf{n}^+ \cdot \nabla \mathbf{b}_1 \cdot \boldsymbol{\tau}) d\Gamma + 2\ell^2 \int_{\Gamma_2} (\tilde{\boldsymbol{\omega}}_{b_2} \cdot \boldsymbol{\tau}) [\mathbf{n}^+ \cdot (\nabla \mathbf{a} + \psi_1 \nabla \mathbf{b}_1) \cdot \boldsymbol{\tau}] d\Gamma \end{aligned} \quad (15f)$$

for any $\boldsymbol{\omega}_a, \boldsymbol{\omega}_{b_1}, \boldsymbol{\omega}_{b_2}, \tilde{\boldsymbol{\omega}}_a, \tilde{\boldsymbol{\omega}}_{b_1}$ and $\tilde{\boldsymbol{\omega}}_{b_2}$ in Ω such that $\boldsymbol{\omega}_a = \boldsymbol{\omega}_{b_1} = \boldsymbol{\omega}_{b_2} = \mathbf{0}$ on Γ_u and $\tilde{\boldsymbol{\omega}}_a \cdot \mathbf{n} = \tilde{\boldsymbol{\omega}}_{b_1} \cdot \mathbf{n} = \tilde{\boldsymbol{\omega}}_{b_2} \cdot \mathbf{n} = \mathbf{0}$ on $\partial\Omega \cup \Gamma_1 \cup \Gamma_2$.”

Equations (15a)-(15c) state equilibrium, whereas equations (15d)-(15f) represent the displacement regularisation. Note that all boundary integrals over cracks Γ_1 and Γ_2 carry a factor 2, the step height in the sign function ψ .

A.2 | Consistent linearisation

Linearisation of the weak form (15) results in the consistent tangent matrix

$$\mathbf{K}_{\text{tan}} = \begin{bmatrix} \mathbf{K}_{\mathbf{a},\mathbf{a}} & \mathbf{K}_{\mathbf{a},\mathbf{b}_1} & \mathbf{K}_{\mathbf{a},\mathbf{b}_2} & \mathbf{K}_{\mathbf{a},\bar{\mathbf{a}}} & \mathbf{K}_{\mathbf{a},\bar{\mathbf{b}}_1} & \mathbf{K}_{\mathbf{a},\bar{\mathbf{b}}_2} \\ \mathbf{K}_{\mathbf{b}_1,\mathbf{a}} & \mathbf{K}_{\mathbf{b}_1,\mathbf{b}_1} & \mathbf{K}_{\mathbf{b}_1,\mathbf{b}_2} & \mathbf{K}_{\mathbf{b}_1,\bar{\mathbf{a}}} & \mathbf{K}_{\mathbf{b}_1,\bar{\mathbf{b}}_1} & \mathbf{K}_{\mathbf{b}_1,\bar{\mathbf{b}}_2} \\ \mathbf{K}_{\mathbf{b}_2,\mathbf{a}} & \mathbf{K}_{\mathbf{b}_2,\mathbf{b}_1} & \mathbf{K}_{\mathbf{b}_2,\mathbf{b}_2} & \mathbf{K}_{\mathbf{b}_2,\bar{\mathbf{a}}} & \mathbf{K}_{\mathbf{b}_2,\bar{\mathbf{b}}_1} & \mathbf{K}_{\mathbf{b}_2,\bar{\mathbf{b}}_2} \\ \mathbf{K}_{\bar{\mathbf{a}},\mathbf{a}} & \mathbf{K}_{\bar{\mathbf{a}},\mathbf{b}_1} & \mathbf{K}_{\bar{\mathbf{a}},\mathbf{b}_2} & \mathbf{K}_{\bar{\mathbf{a}},\bar{\mathbf{a}}} & \mathbf{K}_{\bar{\mathbf{a}},\bar{\mathbf{b}}_1} & \mathbf{K}_{\bar{\mathbf{a}},\bar{\mathbf{b}}_2} \\ \mathbf{K}_{\bar{\mathbf{b}}_1,\mathbf{a}} & \mathbf{K}_{\bar{\mathbf{b}}_1,\mathbf{b}_1} & \mathbf{K}_{\bar{\mathbf{b}}_1,\mathbf{b}_2} & \mathbf{K}_{\bar{\mathbf{b}}_1,\bar{\mathbf{a}}} & \mathbf{K}_{\bar{\mathbf{b}}_1,\bar{\mathbf{b}}_1} & \mathbf{K}_{\bar{\mathbf{b}}_1,\bar{\mathbf{b}}_2} \\ \mathbf{K}_{\bar{\mathbf{b}}_2,\mathbf{a}} & \mathbf{K}_{\bar{\mathbf{b}}_2,\mathbf{b}_1} & \mathbf{K}_{\bar{\mathbf{b}}_2,\mathbf{b}_2} & \mathbf{K}_{\bar{\mathbf{b}}_2,\bar{\mathbf{a}}} & \mathbf{K}_{\bar{\mathbf{b}}_2,\bar{\mathbf{b}}_1} & \mathbf{K}_{\bar{\mathbf{b}}_2,\bar{\mathbf{b}}_2} \end{bmatrix} \quad (16)$$

with the matrices defined in Table 4.

TABLE 4 Block matrices of the consistent tangent matrix.

Secant stiffness matrices, with $\partial\sigma/\partial\varepsilon = (1 - D)C$

$$\mathbf{K}_{\mathbf{a},\mathbf{a}} := \int_{\Omega} \mathbf{B}_{\mathbf{a}}^T (\partial\sigma/\partial\varepsilon) \mathbf{B}_{\mathbf{a}} d\Omega \quad \mathbf{K}_{\mathbf{a},\mathbf{b}_i} = \mathbf{K}_{\mathbf{b}_i,\mathbf{a}}^T := \int_{\Omega} \psi_i \mathbf{B}_{\mathbf{a}}^T (\partial\sigma/\partial\varepsilon) \mathbf{B}_i d\Omega \quad (i = 1, 2) \quad (17a)$$

$$\mathbf{K}_{\mathbf{b}_i,\mathbf{b}_j} := \int_{\Omega} \mathbf{B}_i^T (\partial\sigma/\partial\varepsilon) \mathbf{B}_j d\Omega \quad (i = 1, 2) \quad \mathbf{K}_{\mathbf{b}_1,\mathbf{b}_2} = \mathbf{K}_{\mathbf{b}_2,\mathbf{b}_1}^T := \int_{\Omega} \psi_1 \psi_2 \mathbf{B}_1^T (\partial\sigma/\partial\varepsilon) \mathbf{B}_2 d\Omega \quad (17b)$$

Tangent stiffness matrices, with $\partial\sigma/\partial\bar{\varepsilon} = -C\varepsilon D'(\bar{\gamma}) \frac{\partial\bar{\gamma}}{\partial\bar{\varepsilon}}$

$$\mathbf{K}_{\bar{\mathbf{a}},\bar{\mathbf{a}}} := \int_{\Omega} \mathbf{B}_{\bar{\mathbf{a}}}^T (\partial\sigma/\partial\bar{\varepsilon}) \mathbf{B}_{\bar{\mathbf{a}}} d\Omega \quad \mathbf{K}_{\bar{\mathbf{a}},\bar{\mathbf{b}}_i} = \mathbf{K}_{\bar{\mathbf{b}}_i,\bar{\mathbf{a}}}^T := \int_{\Omega} \psi_i \mathbf{B}_{\bar{\mathbf{a}}}^T (\partial\sigma/\partial\bar{\varepsilon}) \mathbf{B}_i d\Omega \quad (i = 1, 2) \quad (18a)$$

$$\mathbf{K}_{\bar{\mathbf{b}}_i,\bar{\mathbf{b}}_j} := \int_{\Omega} \mathbf{B}_i^T (\partial\sigma/\partial\bar{\varepsilon}) \mathbf{B}_j d\Omega \quad (i = 1, 2) \quad \mathbf{K}_{\bar{\mathbf{b}}_1,\bar{\mathbf{b}}_2} = \mathbf{K}_{\bar{\mathbf{b}}_2,\bar{\mathbf{b}}_1}^T := \int_{\Omega} \psi_1 \psi_2 \mathbf{B}_1^T (\partial\sigma/\partial\bar{\varepsilon}) \mathbf{B}_2 d\Omega \quad (18b)$$

Mass and diffusivity matrices

$$\mathbf{K}_{\bar{\mathbf{a}},\bar{\mathbf{a}}} := -(\mathbf{M} + \ell^2 \mathbf{K}_{\partial\Omega}) \quad \mathbf{K}_{\bar{\mathbf{a}},\mathbf{b}_i} = \mathbf{K}_{\mathbf{b}_i,\bar{\mathbf{a}}}^T := -(\mathbf{M}_{\psi_i} + \ell^2 \mathbf{K}_{\partial\Omega,\psi_i} + 2\ell^2 \mathbf{K}_{\Gamma_i}) \quad (i = 1, 2) \quad (19a)$$

$$\mathbf{K}_{\bar{\mathbf{b}}_i,\bar{\mathbf{b}}_j} := -(\mathbf{M} + \ell^2 \mathbf{K}_{\partial\Omega}) \quad (i = 1, 2) \quad \mathbf{K}_{\bar{\mathbf{b}}_1,\bar{\mathbf{b}}_2} = \mathbf{K}_{\bar{\mathbf{b}}_2,\bar{\mathbf{b}}_1}^T := -(\mathbf{M}_{\psi_1\psi_2} + \ell^2 \mathbf{K}_{\partial\Omega,\psi_1\psi_2} + 2\ell^2 \mathbf{K}_{\Gamma_1,\psi_2} + 2\ell^2 \mathbf{K}_{\Gamma_2,\psi_1}) \quad (19b)$$

$$\mathbf{K}_{\bar{\mathbf{a}},\bar{\mathbf{a}}} := \mathbf{M} + \ell^2 \mathbf{D} \quad \mathbf{K}_{\bar{\mathbf{a}},\bar{\mathbf{b}}_i} = \mathbf{K}_{\bar{\mathbf{b}}_i,\bar{\mathbf{a}}}^T := \mathbf{M}_{\psi_i} + \ell^2 \mathbf{D}_{\psi_i} \quad (i = 1, 2) \quad (19c)$$

$$\mathbf{K}_{\bar{\mathbf{b}}_i,\bar{\mathbf{b}}_j} := \mathbf{M} + \ell^2 \mathbf{D} \quad (i = 1, 2) \quad \mathbf{K}_{\bar{\mathbf{b}}_1,\bar{\mathbf{b}}_2} = \mathbf{K}_{\bar{\mathbf{b}}_2,\bar{\mathbf{b}}_1}^T := \mathbf{M}_{\psi_1\psi_2} + \ell^2 \mathbf{D}_{\psi_1\psi_2} \quad (19d)$$

Some remarks about the matrices in Table 4:

- Equation (17) shows the secant stiffness matrices. $\mathbf{K}_{\mathbf{a},\mathbf{a}}$ is the standard secant matrix of the continuous model, whereas the enriched secant matrices $\mathbf{K}_{\mathbf{a},\mathbf{b}_1}$ and $\mathbf{K}_{\mathbf{b}_1,\mathbf{b}_1}$ are the ones already obtained for the single-crack. Matrices $\mathbf{K}_{\mathbf{a},\mathbf{b}_2}$ and $\mathbf{K}_{\mathbf{b}_2,\mathbf{b}_2}$ are these same matrices for the secondary crack. The interaction between the two cracks is represented by $\mathbf{K}_{\mathbf{b}_1,\mathbf{b}_2}$. A similar comment applies to the tangent stiffness matrices of Equation (18).
- In equations (17) and (18), $\mathbf{B}_{\mathbf{a}}$, \mathbf{B}_i and \mathbf{B}_2 are the usual matrices of shape function derivatives. Note that the dimen-

sions of \mathbf{B}_a are fixed, because ndof does not change, whereas the dimensions of \mathbf{B}_1 and \mathbf{B}_2 change throughout the simulation, because ndofEnr1 and ndofEnr2 grow as the cracks propagate.

- Equation (19) shows the matrices associated to displacement smoothing. \mathbf{M} and \mathbf{D} are standard mass and diffusivity matrices,

$$\mathbf{M} := \int_{\Omega} \mathbf{N}^T \mathbf{N} d\Omega \quad , \quad \mathbf{D} := \int_{\Omega} \nabla \mathbf{N}^T \nabla \mathbf{N} d\Omega \quad (20)$$

where \mathbf{N} contains shape functions and $\nabla \mathbf{N}$ their gradients. The enriched matrices \mathbf{M}_{ψ_1} , \mathbf{D}_{ψ_1} , \mathbf{M}_{ψ_2} , \mathbf{D}_{ψ_2} , $\mathbf{M}_{\psi_1\psi_2}$ and $\mathbf{D}_{\psi_1\psi_2}$ take into account the discontinuities. For instance,

$$\mathbf{M}_{\psi_1} := \int_{\Omega} \psi_1 \mathbf{N}^T \mathbf{N} d\Omega \quad , \quad \mathbf{D}_{\psi_1\psi_2} := \int_{\Omega} \psi_1 \psi_2 \nabla \mathbf{N}^T \nabla \mathbf{N} d\Omega \quad (21)$$

- Matrices $\mathbf{K}_{\partial\Omega}$, \mathbf{K}_{Γ_1} , \mathbf{K}_{Γ_2} in equation (19), and their enriched versions $\mathbf{K}_{\partial\Omega,\psi_1}$, $\mathbf{K}_{\partial\Omega,\psi_2}$, $\mathbf{K}_{\partial\Omega,\psi_1\psi_2}$, $\mathbf{K}_{\Gamma_1,\psi_2}$, $\mathbf{K}_{\Gamma_2,\psi_1}$ account for the tangential component of the boundary condition, equation (1i). For instance,

$$\mathbf{K}_{\partial\Omega} := \int_{\partial\Omega} \mathbf{N}^T \mathbf{c} \nabla \mathbf{N} d\Gamma \quad , \quad \mathbf{K}_{\Gamma_1,\psi_2} := \int_{\Gamma_1} \psi_2 \mathbf{N}^T \mathbf{c} \nabla \mathbf{N} d\Gamma \quad \text{with} \quad \mathbf{c} = \begin{bmatrix} n_x \tau_x^2 & n_y \tau_x^2 & n_x \tau_x \tau_y & n_y \tau_x \tau_y \\ n_x \tau_x \tau_y & n_y \tau_x \tau_y & n_x \tau_y^2 & n_y \tau_y^2 \end{bmatrix} \quad (22)$$

- To compact the notation in equations (19)-(22), the subscript (a , 1 or 2) is dropped from matrices \mathbf{N} and $\nabla \mathbf{N}$, whose dimensions should be understood from the context. With this abuse of notation, matrices $\mathbf{K}_{\bar{a},\bar{a}}$, $\mathbf{K}_{\bar{b}_1,\bar{b}_1}$ and $\mathbf{K}_{\bar{b}_2,\bar{b}_2}$, for instance, have dimensions $\text{ndof} \times \text{ndof}$, $\text{ndofEnr1} \times \text{ndofEnr1}$ and $\text{ndofEnr2} \times \text{ndofEnr2}$ respectively, whereas matrix $\mathbf{K}_{\bar{b}_1,\bar{b}_2}$ has dimensions $\text{ndofEnr1} \times \text{ndofEnr2}$.
- The size of the global tangent matrix (16) increases from a fixed 2ndof in the continuous regime to a varying $2(\text{ndof} + \text{ndofEnr1} + \text{ndofEnr2})$ in the discontinuous regime. For the typical case of $\text{ndof} > \{\text{ndofEnr1}, \text{ndofEnr2}\}$, however, this represents only a moderate increase in the system size.

Due to X-FEM enrichment, the computation of matrices and vectors involves the computation of discontinuous functions (see, for instance, all the matrices in Table 4 with sign functions ψ_1 , ψ_2 or both). In this work, the cracked quadrilateral is divided into two polygonal subelements (three for the case of a branching crack) that are further divided into triangles, see figure 14. Each triangle subdomain is mapped into the parent unit triangle over which a standard Gaussian quadrature is used. This subdivision into triangles may be avoided by using alternative strategies, such as the equivalent polynomial approach of Ventura and Benvenuti [52].

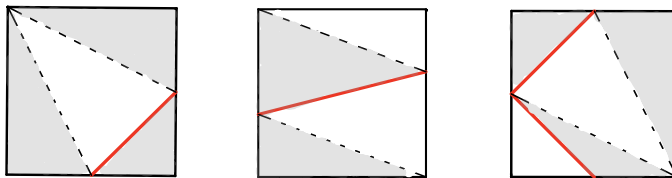


FIGURE 14 X-FEM numerical integration: subdivision of finite elements with one or two cracks into triangles.